Universidade de Brasília

Faculdade de Tecnologia

Departamento de Engenharia Elétrica

NGSO-to-GSO Satellite Systems Interference Mitigation in Ku Band

Luciana Rabelo Novato Ferreira

DISSERTAÇÃO DE MESTRADO

ENGENHARIA ELÉTRICA

Brasília

2026

Universidade de Brasília
Faculdade de Tecnologia
Departamento de Engenharia Elétrica

NGSO-to-GSO Satellite Systems Interference Mitigation in Ku Band

Luciana Rabelo Novato Ferreira

Dissertação de Mestrado submetida ao Programa de Pós-Graduação em Engenharia Elétrica da Universidade de Brasília como parte dos requisitos necessários para obtenção do grau de Mestre.

Orientador: Prof. Dr. Hugerles S. Silva
Coorientadores: Prof. Dr. Higo Thaian Pereira da Silva e Prof. Dr. Paulo H. P. de Carvalho

Brasília
2026

FICHA CATALOGRÁFICA

FERREIRA, LUCIANA RABELO NOVATO

NGSO-to-GSO Satellite Systems Interference Mitigation in Ku Band. [Brasília] 2026.

xvii, 64 p., 210 x 297 mm (ENE/FT/UnB, Mestre, Dissertação de Mestrado – Universidade de Brasília. Faculdade de Tecnologia).

Departamento de Engenharia Elétrica.

1. Controle de potência
2. Direcionamento de feixe
3. GEO
4. NGEO
5. Mitigação de Interferência
I. ENE/FT/UnB
II. Título (série)

REFERÊNCIA BIBLIOGRÁFICA:

FERREIRA, L. R. N. (2026). NGSO-to-GSO Satellite Systems Interference Mitigation in Ku Band. Dissertação de Mestrado em Engenharia Elétrica, Publicação PPGEE 839/26, Departamento de Engenharia Elétrica, Universidade de Brasília, Brasília, DF, 64 p.

Luciana Rabelo Novato Ferreira
Universidade de Brasília (UnB)
Campus Darci Ribeiro
Faculdade de Tecnologia - FT
Departamento de Engenharia Elétrica (ENE)
Brasília, DF - CEP 70919-970

Universidade de Brasília
Faculdade de Tecnologia
Departamento de Engenharia Elétrica

NGSO-to-GSO Satellite Systems Interference Mitigation in Ku Band

Luciana Rabelo Novato Ferreira

Dissertação de Mestrado submetida ao Programa de Pós-Graduação em Engenharia Elétrica da Universidade de Brasília como parte dos requisitos necessários para obtenção do grau de Mestre.

Trabalho aprovado. Brasília, 13 de março de 2026:

Prof. Dr. Hugerles S. Silva
UnB/FT/ENE
Orientador

Prof. Dr. Renato Alves Borges
UnB/FT/ENE
Examinador interno

Prof. Dr. Robson Domingos Vieira
UnB/FT/ENE
Examinador interno, suplente

Dr. Agostinho Linhares de Souza Filho
IPE Digital
Examinador externo

Este trabalho é dedicado às mulheres que,
quando crianças, sonharam em ser Engenheiras e,
quando adultas, persistiram até conquistarem o seu sonho.

Agradecimentos

Inicialmente, gostaria de agradecer aos engenheiros da minha vida. Aos meus pais, Isoilda e Oromar, engenheiros formados na UnB, por me guiarem desde pequena e serem os maiores responsáveis pela pessoa que eu me tornei hoje.

Ao meu marido Yroá, também Engenheiro Eletricista, por ser o melhor companheiro de vida que eu poderia ter, por todo o amor, carinho e paciência, meu porto seguro e o meu suporte em todos os momentos.

A minha filha, Isadora, por ser um doce de menina e por ser tão compreensiva com a mãe que a ama tanto e que nem sempre está presente para compartilhar todos os momentos de sua vida.

Ao meu irmão Guilherme e a minha cunhada Rose, que mesmo distante, sei que sempre estão torcendo pelo meu sucesso.

E claro, ao meu orientador e co-orientadores, Prof. Hugerles, Prof. Higo e Prof. Paulo, por toda direção, tempo e esforço para me ajudarem a chegar até aqui, Mestre em Engenharia Elétrica na área de Satélites, tema em que decidi, já há muitos anos, dedicar a minha vida. Foi uma honra ter sido guiada por vocês nessa longa jornada, muito obrigada!

“If you find that you’re spending almost all your time on theory,
start turning some attention to practical things;
it will improve your theories.
If you find that you’re spending almost all your time on practice,
start turning some attention to theoretical things;
it will improve your practice.”
(Donald Knuth)

Resumo

Mitigação de Interferências entre Sistemas por Satélite NGEO e GEO em Banda Ku

Esse trabalho investiga o uso combinado de técnicas de controle de potência e direcionamento de feixe de antena para mitigar interferências entre sistemas de satélites em órbitas não geoestacionárias (NGEO) e satélites em órbitas geoestacionárias (GEO) na banda Ku. O resultado das simulações, que considera características de constelações reais e segue recomendações da União Internacional de Telecomunicações (UIT), estão presentes sob diversas configurações de sistema. As análises apresentadas neste trabalho não foram identificadas na literatura, constituindo uma nova abordagem para mitigar interferências, garantindo que a densidade de fluxo de potência equivalente (EPFD) do sistema NGEO atenda aos limites regulatórios da UIT.

Palavras-chave: Controle de potência; Direcionamento de feixe; GEO; NGEO; Mitigação de Interferência.

Abstract

This work investigates the jointly use of power control and beam steering techniques to mitigate interference between non-geostationary satellite orbit (NGSO) and geostationary satellite orbit (GSO) systems operating in the Ku band. Simulation results, which consider realistic NGSO system characteristics and follow International Telecommunication Union (ITU) recommendations, are presented under various system configurations. The analyses conducted in this study have not been identified in the literature and therefore constitute a novel approach to interference mitigation, ensuring that the equivalent power flux-density (EPFD) of NGSO systems complies with ITU regulatory limits.

Keywords: Power control; Beam Steering; GSO; NGSO; Interference Mitigation.

List of figures

List of tables

List of acronyms and symbols

List of Acronyms

1D	One-dimensional
2D	Two-dimensional
3GPP	3rd Generation partnership project
6G	Six generation of mobile networks
ABNT	Associação Brasileira de Normas Técnicas
AE	Autoencoder
AI	Artificial intelligence
BS	Beam steering
C-PC	Cognitive range-based power control
C/I	Carrier-to-interference ratio
CAE	Convolutional autoencoder
CNN	Convolutional neural network
CR	Cognitive radio
DRL	Deep reinforcement learning
DSA	Dynamic spectrum access
EDRL-FBAM	Event-driven deep RL-based frequency band allocation mechanism
EIRP	Equivalent isotropically radiated power
EPFD	Equivalent power flux density
ESA	European Space Agency
FFT	Fast Fourier transform
GSO	Geostationary satellite orbit system
I/N	Interference-to-noise ratio
I/Q	In-phase/quadrature
INPI	Instituto Nacional da Propriedade Industrial
IoT	Internet of things
ISD	Inter-Site distance
ITU	International Telecommunications Union
LEO	Low Earth orbit
LoS	Line-of-sight
MAE	Mean average error
MIMO	Multiple-input multiple-output
MISO	Multiple-input single-output
ML	Machine learning
NGSO	Non-geostationary satellite orbit system

NOMA	Non-orthogonal multiple access
PC	Power control
R-PC	Range-based power control
RIS	Reconfigurable intelligent surface
RL	Reinforcement learning
RR	ITU-R Radio Regulations
RSMA	Rate-splitting multiple access
SINR	Signal-to-interference-plus-noise ratio
SLNR	Signal-to-leakage-plus-noise ratio
SLR	Signal-to-leakage ratio
TA-PC	Traffic-aware power control
TrID	Transformer-based interference detector
UIT	União Internacional de Telecomunicações
UIT-R	Bureau de radiocomunicações da UIT
UnB	Universidade de Brasília
VAE	Variational autoencoder
WCG	Worst-case geometry

List of Symbols

$2\Delta\alpha$	Angular span of the arc with respect to the Earth's center
$2\Delta\beta$	Angular width of the GSO satellite antenna
$2\Delta\vartheta$	Mitigation zone angle
$\bar{\varphi}$	Beam steering angle
$\bar{G}_{\text{rx}}$	GSO earth stations maximum gain
$\bar{G}_{\text{tx}}$	Maximum gain of the NGSO satellites
$\Delta\theta$	Angle between satellites in an orbital plan
δ_{tx}	Antenna aperture size in wavelengths
κ	Power Control level
λ	Wavelength
$\langle\cdot,\cdot\rangle$	Dot product operator
$\mathbf{e}(\alpha)$	Main beam vector of the ground stations antennas
$\mathbf{g}$	Position vector of the GSO satellite
$\mathbf{r}(\alpha)$	Positions of the GSO ground stations
$\mathcal{S}_{\nu}(\alpha)$	Set of visible NGSO satellites at position α
$\mathcal{S}_{\text{a}}(\alpha)$	Subset of visible satellites inside the interference mitigation zone
μ_k	k-th zero of $J_1(\cdot)$
ρ_{s}	Satellite density
σ	Beam broadening factor

φ	Observation angle relative to the antenna's boresight (main lobe axis)
φ'	Angle between the boresight vector $\mathbf{e}(\alpha)$ and the vector $\mathbf{x}_n$
φ_n	Angle between boresight vector $\mathbf{b}_n$ and $-\mathbf{x}_n$
A	Parameter related to sidelobe level in Taylor model
$B_{\text{w;ref}}$	Reference bandwidth
$d_n(\alpha)$	Distance between the earth station and the n-th visible satellite
h_{GSO}	Altitude of the GSO satellite
h_{NGSO}	Altitude of the NGSO satellites
$J_1(\cdot)$	First-order Bessel function of the first kind
K	Number of sidelobes
l_{c}	Lenth of the GSO coverage arc
N	Total number of NGSO satellites
N_{p}	Number of orbital planes
N_{sp}	Number of NGSO satellites in a orbital plane
N_{s}	Number of satellites in a orbital plan
P_{t}	Power at the input of the antenna of the transmit station, considered in the NGSO system (dBW) in the reference bandwidth
R_{e}	Earth's radius
S	Sidelobe level
s_{n}	Positions of the NGSO satellites
u_{k}	Parameter used in Taylor antenna model
x_{n}	Vector from ground station to satellite

Contents

1 Introduction

1.1 Scope and Related Works

Since the beginning of the space age, geostationary satellite orbit (GSO) systems have been used for international communications due to their fixed position relative to the Earth's surface, which allows continuous coverage over specific regions. However, increased demand for satellite-based services and the growing number of GSO satellites have raised concerns about potential congestion of the GSO arc [1]. To address these limitations and enhance global connectivity, non-geostationary satellite orbit (NGSO) systems began to be developed in 1990s. With the emergence NGSO systems, concerns regarding potential interference affecting the operation of existing GSO networks have arisen. As a result, the International Telecommunication Union (ITU) approved Article 22 of the Radio Regulations (RR) – Space Services [2], that establishes equivalent power flux-density (EPFD) limits that must be respected by NGSO systems in order to protect GSO operations.

Over the years, NGSO systems have become a trend and a number of large NGSO constellations have started to be launched [3]. Due to this, several studies on the coexistence of GSO and NGSO systems have been described in the literature [4–8]. For example, the authors in [4] present a study on interference in the Ku band between satellite systems. The work evaluates the impact of interference on throughput degradation, considering heterogeneous satellite constellations and the look-aside and band-splitting interference mitigation techniques. The downlink interference between low Earth orbit (LEO) and GEO systems in Ka band is studied in [5] and the impact of use the exclusion angle strategy, on the in-line downlink interference and the coverage of LEO system, is analyzed considering the OneWeb constellation.

The authors in [6] conducted a study on the interference of LEO systems on GEO satellite systems that share the same Ku band. Furthermore, the study estimates the probability of interference events based on real-world parameters of constellations such as Starlink and OneWeb, and proposes the use of beam steering (BS) as a practical and effective approach to mitigate the interference between the systems. The authors in [7] analyze the effects of LEO satellite antenna sidelobe radiation on GEO satellite ground stations, even when BS techniques are employed to prevent the main beams from reaching these stations. In [7], the limits imposed by the ITU Radio Regulations for EPFD are studied and the maximum limits for the levels of sidelobes that LEO constellations must respect are proposed. In [8], a study on the inter-system downlink interference of NGSO systems on GSO ground stations is presented, considering the scenario of co-located stations. The mentioned work proposes a new visibility analysis approach to model the interference more efficiently. In addition, the

interference is evaluated through detailed simulations considering the Starlink constellation, that contains more than 4000 satellites.

1.2 Objectives

The objective of this work is to investigate and develop an effective interference mitigation strategy to enable the spectral coexistence between NGSO and GSO systems operating in the Ku band. Specifically, the work aims to analyze and validate the joint application of power control (PC) and BS techniques within a predefined mitigation zone, ensuring that the equivalent power flux density (EPFD) generated by NGSO systems remains within the regulatory limits established by ITU. By considering wost-case geometry (WCG) conditions and realistic NGSO system parameters, the study seeks to propose a low-complexity and scalable solution capable of protecting GSO earth stations while preserving the operational performance and coverage of NGSO systems.

1.3 Original Contributions

This document is based on the work presented in papers published in the field of this dissertation. It contains original contributions to the state-of-the-art, namely:

- Chapter 3 presents: (i) a low-complexity method that jointly applies PC and BS within a defined angular mitigation zone; (ii) an expression that defines the equivalent angle at Earth's center of the GSO satellite antenna beam width and (iii) the EPFD formula modified that incorporates PC and BS approaches.
- Chapter 4 extends the analysis of Chapter 3 to a more realistic system model with the NGSO satellites positions determined by Recommendation ITU-R S.1503-4 [9] and the GSO earth stations distributed in a circular footprint area.

1.4 Publications and Softwares

1. L. R. N. Ferreira, H. S. Silva, H. T. P. Silva, and P. H. P. de Carvalho, Joint Power Control and Beam Steering for NGSO-to-GSO Interference Mitigation in Ku Band. *SBMO/IEEE MTT-S International Microwave and Optoelectronics Conference (IMOC)*, pp. 1-5, Nov. 2025.
2. L. R. N. Ferreira, H. S. Silva, H. T. P. Silva, and P. H. P. de Carvalho, "Certificado de Registro de Programa de Computador," Título: Joint Power Control and Beam Steering for NGSO-to-GSO Interference Mitigation in Ku Band, Linguagem: Python, Campo de aplicação: TC0-2, Tipo de Programa: SM-01 , Processo No: BR512025005196-4, Instituto Nacional de Propriedade Intelectual (INPI), Data da expedição: 21 de outubro de 2025.

3. L. R. N. Ferreira, H. S. Silva, H. T. P. Silva, and P. H. P. de Carvalho, Spectral Coexistence Between NGSO and GSO Satellite Systems: A Recent Survey. *IEEE Access*, Under review, pp 1-9, Jan. 2026.
4. L. R. N. Ferreira, H. S. Silva, H. T. P. Silva, and P. H. P. de Carvalho, Joint Power Control and Beam Steering for NGSO-to-GSO Interference Mitigation in Ku Band: A New Approach. In preparation, pp. 1-9, Feb. 2026.
5. L. R. N. Ferreira, H. S. Silva, H. T. P. Silva, and P. H. P. de Carvalho, "Certificado de Registro de Programa de Computador," Título: Joint Power Control and Beam Steering for NGSO-to-GSO Interference Mitigation in Ku Band: A New Approach, Linguagem: Python, Campo de aplicação: TC0-2, Tipo de Programa: SM-01 , Processo No: BR512026001688-6, Instituto Nacional de Propriedade Intelectual (INPI), Data da expedição: 24 de março de 2026.

1.5 Document Organization

This document is organized as follows. Chapter 2 presents a recent review of interference mitigation technique, including PC and BS. Chapter 3 describes a simplified system model, the corresponding interference analysis, and the mitigation techniques considered, together with details of the simulation setup and the corresponding numerical results. Chapter 4 introduces a more realistic system model, in which the same mitigation techniques presented in Chapter 3 are employed, and reports the numerical results obtained. Finally, Chapter 5 concludes the dissertation by summarizing the main findings of this study.

2 Spectral Coexistence Between NGSO and GSO Satellite Systems: A Recent Survey

The rapid expansion of NGSO systems has reshaped the role and deployment strategies of traditional GSO satellites and the recent NGSO systems. Considering that, several studies in this area have investigated interference mitigation solutions. In this context, this chapter aims to provide a recent overview of the state of the art on interference mitigation and detection between GSO and NGSO satellite systems. Besides, it outlines the associated challenges and directions for future research in sustainable multi-orbit satellite networks. Based on the literature review, interference mitigation techniques can be grouped into two main classes: non-cooperative strategies and cooperative.

2.1 Non-Cooperative Interference Mitigation Strategies

A non-cooperative strategy is defined as an approach in which the NGSO system adapts its operation independently, without requiring synchronization or coordination with the GSO system. Recent research on non-cooperative strategies encompasses the following techniques: exclusion angle, PC, beamforming and beam-tilting, movable antennas, and reinforcement learning (RL)–based approaches. The most recent applications of these techniques are reviewed in the following subsections. These techniques are not mutually exclusive and may be jointly applied to enhance the efficiency of interference mitigation. The combined use of non-cooperative strategies is discussed in Subsection 2.1.6. For a clearer overview, Fig. 2.1 presents a graphical timeline summary of the publications addressing each non-cooperative technique discussed in this section. In this figure, the references in blue are the ones related to a single interference mitigation technique and, in red, the ones with a joint approach.

2.1.1 Exclusion Angle

The exclusion angle is a technique that partially or completely restricts the operation of NGSO satellites when they are located within a predefined angular region, aiming to reduce interference to the GSO system, as shown in Fig. 2.2. In [10], this technique is applied to mitigate interference between GSO and NGSO systems operating in the Ka band, with ranges from 17 GHz to 30 GHz. Simulation results demonstrate that larger exclusion angles (*e.g.*,

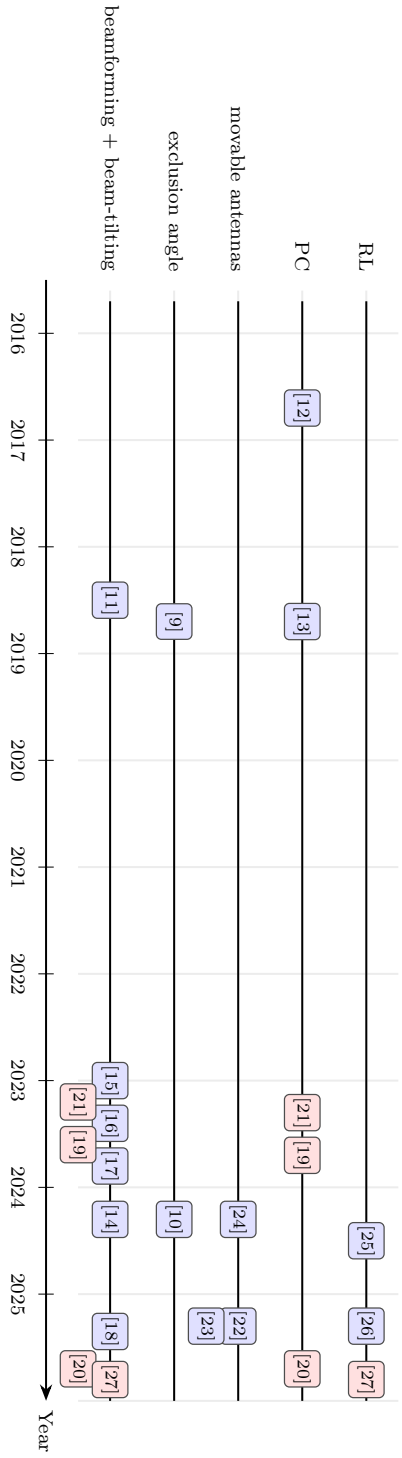

Figure 2.1 – Timeline of publications on non-cooperative mitigation techniques.

8°, 10°, and 12°) significantly reduce EPFD levels at GSO terminals, effectively suppressing harmful in-line interference. However, this approach introduces significant trade-offs: while interference is mitigated, NGSO coverage is reduced, leading to non-communication zones whose extent depends on the latitude of the GSO earth stations.

A complementary analysis of Ka-band interference mitigation using exclusion angles

is presented in [11]. Through a simulation framework, carrier-to-interference (C/I) ratio statistics are evaluated while accounting for atmospheric effects such as rain attenuation. Two key coexistence parameters are investigated: the exclusion angle around GSO links and the maximum number of co-frequency NGSO satellites transmitting near a GSO ground station. The results show that increasing the exclusion angle or reducing the number of co-frequency NGSO satellites mitigate interference, thereby improving coexistence strategies between NGSO and GSO systems.

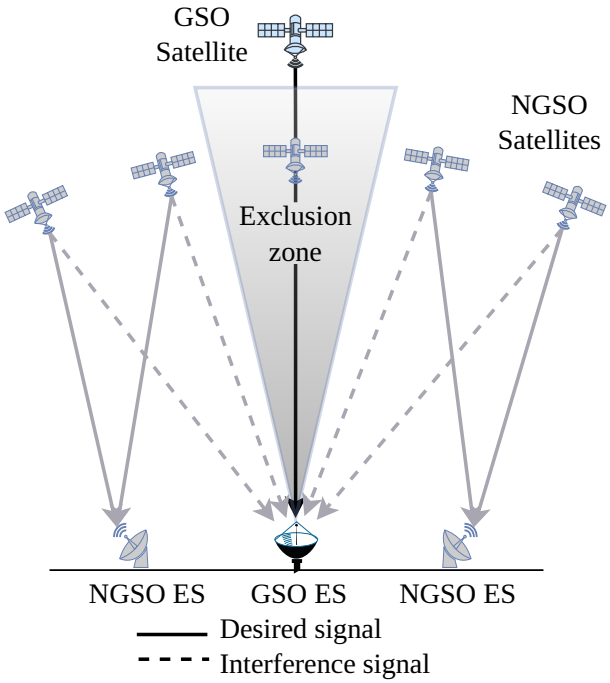

Figure 2.2 – Exclusion angle representation, in which ES is the earth stations of each satellite system.

2.1.2 Power Control

In PC-based approaches, the transmission power of interfering satellites is dynamically adjusted to meet the protection requirements of the victim system [12]. In [13], the authors present a study on spectral coexistence with particular emphasis on in-line interference events, that is, situations where an NGSO satellite crosses the line-of-sight (LoS) path of a GSO earth link. To address this issue, several strategies are proposed, including range-based PC (R-PC), in which the NGSO satellite's transmit power is adjusted according to its distance from the terrestrial terminal. Moreover, the authors introduce an optimization-based methodology to determine the minimum inter-site distance (ISD) between GSO and NGSO earth terminals, aiming to minimize interference while maximizing spectral efficiency.

Another PC-based approach is presented in [14], which proposes a successive convex approximation-based power allocation scheme for coordinated multi-satellite systems employing full frequency reuse, zero-forcing precoding, and user scheduling. The objective is

to maximize the total system capacity under transmission power constraints, formulated as a non-convex optimization problem. The successive convex approximation method is applied to transform the non-convex objective function into a series of convex subproblems via logarithmic approximation, which are then solved using the Lagrangian dual method. Simulation results demonstrate that the proposed scheme substantially enhances total capacity compared to scenarios without power allocation and outperforms the classical iterative water-filling method in terms of achievable capacity and convergence speed. The integrated performance analysis further shows that combining semi-orthogonal user selection with the proposed power allocation yields the highest total system capacity.

2.1.3 Beamforming and Beam-tilting

A straightforward strategy for mitigating interference is beamforming, as illustrated in Fig. 2.3. In this technique, the NGSO satellites adjust their antenna radiation patterns to dynamically suppress interference [15]. Several studies apply beamforming techniques, either alone or in combination with another approach. In [15], a review of beamforming in interference management is presented, where it is emphasized that advanced beamforming techniques are fundamental to enable scalable and interference-resilient NGSO deployments, reinforcing their critical role in the evolution of dense satellite communication networks.

Interference issues in NGSO systems caused by the beam spillover effect is investigated in [16]. This effect occurs when the projected satellite beams overlap on Earth due to satellite motion and geometry. This overlap can lead to interference between gateway (feeder link) and user downlink beams, especially when both operate within the same band. The study presents link budget analyses and propose an adaptive beamforming technique with null-steering, which suppresses interference by placing signal nulls toward victim receivers. Simulation results based on a NGSO scenario demonstrate that the proposed beam-nulling method significantly improves the carrier-to-interference (C/I) maintaining above operational thresholds. A similar simulation is done in [17], showing that the method significantly reduces the interference-to-noise (I/N) ratio at GSO receivers. Both studies conclude that adaptive beamforming is a promising strategy to ensure spectrum coexistence in future high-throughput NGSO systems.

The authors in [18] propose a dynamic interference mitigation method for NGSO satellite systems with adaptive beamforming added by sidelobe level control to reduce co-frequency interference. Using a uniform rectangular array antenna and the Taylor weighting algorithm, this approach adjusts the antenna beam pattern in real time according to the relative positions of interfering and serving satellites. By selecting an optimal sidelobe control, the system minimizes interference while maintaining communication performance. Simulation based on Starlink and OneWeb constellation models show that the proposed method improves the C/I by 47.5% compared to conventional techniques, achieving C/I

values above 27 dB for 95% of the time and increasing the maximum C/I from 40 dB to 80 dB and conclude that adaptive beamforming with sidelobe suppression significantly enhances NGSO satellite systems' robustness and reliability in shared-spectrum environments.

The study presented in [19] proposes a novel interference avoidance strategy for NGSO systems based on transmit beamforming to address spectrum coexistence challenges in NGSO systems, particularly in collinear scenarios with GSO and other NGSO satellites. The approach models both inter-system (NGSO to GSO/NGSO) and intra-system interference constraints by transforming them into gain constraints for transmitting beams. An enhanced linearly constrained minimum variance algorithm, which incorporates eigenvalue decomposition and singular value decomposition, is developed to solve the resulting non-convex optimization problem by creating nulls in the transmit beam pattern at collinear points. Simulation results, using actual Starlink and GSO system data, validate the strategy's effectiveness, showing a significant reduction in interference (EPFD for GSO and I/N for NGSO) and a substantial decrease in the required isolation angle, which in turn increases the NGSO system services range.

Another interference mitigation approach based on the radiation pattern of NGSO antennas is beam-tilting. In the study presented in [20], interference mitigation is achieved by tilting the phased-array antennas of NGSO satellites. This adjustment increases the angular separation between the NGSO and GSO links, thereby reducing harmful in-line interference. The results indicate that spectral coexistence can be achieved without modifying the constellation architecture, with earth stations located in low-latitude regions benefiting the most.

2.1.4 Movable Antennas

Unlike conventional fixed-position antenna arrays, movable antennas allows each element to physically adjust, providing extra degrees of freedom for beam pattern adaptation to time-varying user distributions. The work presented in [21] introduces a novel mitigation strategy using movable antennas for spectrum sharing between NGSO and GSO systems. The problem is formulated as a max-min signal-to-interference-plus-noise ratio (SINR) optimization, constrained by interference thresholds for GSO links. To address the resulting highly non-convex problem, the authors propose an alternating optimization algorithm that jointly optimizes signal-to-leakage-plus-noise ratio (SLNR) precoding, power allocation, and antenna positions, employing simulated annealing to refine placement. The findings demonstrate that movable antennas, combined with advanced precoding and PC, provide an effective and robust solution for balancing NGSO service quality with coexistence requirements.

In [22] and [23], a similar approach is presented, demonstrating that movable antennas based in beamforming significantly decreases interference leakage and improves the signal-

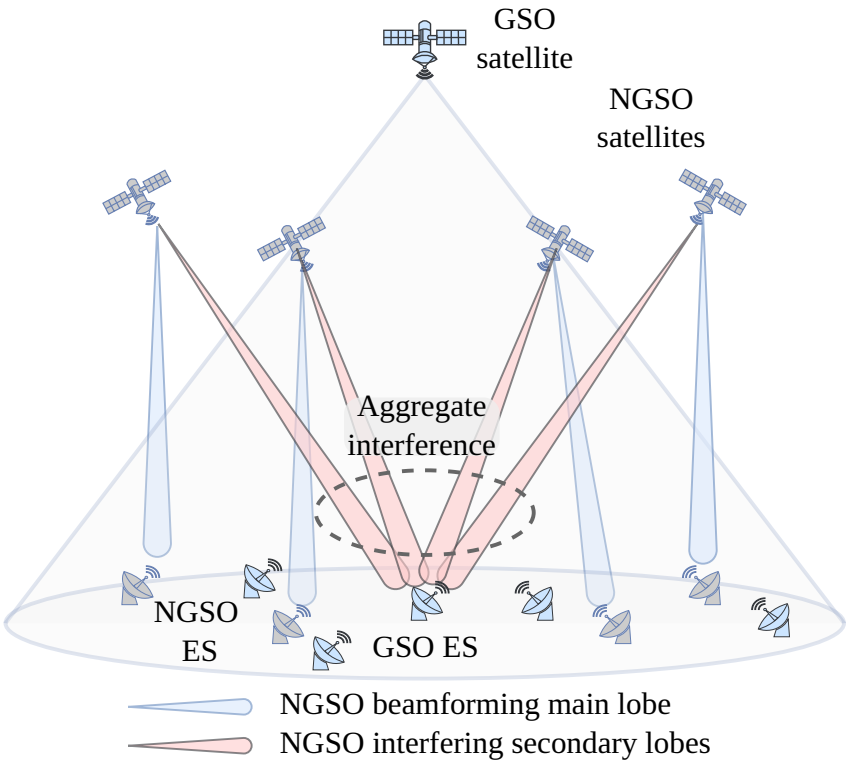

Figure 2.3 – Beamforming representation.

to-leakage ratio (SLR) compared to traditional arrays, offering an effective and feasible solution for next-generation satellite communication networks.

2.1.5 Reinforcement Learning

RL is a machine learning paradigm in which an agent learns to make sequential decisions by interacting with an environment, in order to maximize a cumulative reward over time. Due to its flexibility and effectiveness in automating decision-making, RL has been applied to managing interference between GSO and NGSO systems. The authors in [24] formulate the spectrum interference challenges in GSO-NGSO co-existing satellite networks as a nonlinear programming problem, aimed at maximizing the average binary scale satisfaction of NGSO satellites while ensuring the GSO satellite's data rate requirements. To solve this, the study proposes an event-driven deep RL-based frequency band allocation mechanism (EDRL-FBAM), leveraging proximal policy optimization to dynamically manage spectrum allocation in response to stochastic NGSO requests. Simulations demonstrate that EDRL-FBAM significantly outperforms random allocation strategies by improving the average data rates of NGSO and GSO satellites as well as enhancing NGSO quality of service.

Another proposal is presented in [25], in which is studied a case where multiple satellites share limited spectrum resources without direct coordination. The authors model the dynamic downlink interference problem as a multi-armed bandit optimization, leveraging RL algorithms such as upper confidence bound and Thompson sampling. To overcome the

high learning complexity caused by large user populations and short satellite contact times, a hierarchical information structure is introduced, which aggregates information at the user level to reduce the state space and computational cost. Simulation results show that the hierarchical approach significantly improves throughput and reduces collision rates compared to baseline and user-based models, achieving near-optimal performance even under dense user scenarios.

2.1.6 Joint Techniques

In the literature, studies demonstrate that using joint implementation of interference mitigation strategies significantly enhances overall effectiveness. For instance, in [12] it is proposed a joint power and tilt control strategy to mitigate interference while maximizing user experience within the NGSO constellations. This approach ensures that the EPFD of NGSO systems remains within the ITU regulatory limits and optimizes radio resource management for user services. The method combines PC with satellite tilting and introduces a heuristic solution to minimize the number of satellites requiring adjustment. By identifying and tilting only the critical satellites, the approach reduces operational complexity and computational load while maintaining comparable demand satisfaction levels.

In [26], the authors present an alternative to PC, combining BS with control of the sidelobe levels of the antennas. The aforementioned study examines how NGSO sidelobe radiation can generate harmful interference to GSO systems, even when the main beam is steered away from GSO ground stations. Simulations evaluate maximum permissible sidelobe levels for Ku-band constellations, focusing on Starlink and OneWeb as case studies. The results show that sidelobe suppression requirements depend on constellation altitude, equivalent isotropic radiated power (EIRP), and size, with larger constellations necessitating stricter control. In [27] it is presented a low-complexity method that jointly applies PC and BS within a defined angular mitigation zone. In BS, the angle of the interfering radiation pattern is modified with the aim of mitigating or avoiding in-line events. Unlike solutions that require strict synchronization, the strategy shown in [27] relies solely on geometric parameters accessible to both NGSO and GSO systems. Simulations consider ITU recommendations and real-world constellation parameters such as altitude, number of satellites, and antenna characteristics. Results indicate that using PC or BS individually is insufficient to satisfy strict ITU EPFD limits. However, their combination ensures compliance and effective protection of GSO ground stations.

The study in [28] introduces a joint optimization approach that combines beam management, including BS and beamwidth control; with dynamic resource allocation across time, frequency, and space domains. By formulating the problem as a non-convex mixed-integer optimization, the authors employ a deep RL algorithm to efficiently adapt beam configurations and spectrum assignments in response to time-varying interference and

Table 2.1 – Summary of non-cooperative interference mitigation techniques

Technique	Working Principle	Required Information	Implementation	Advantages	Limitations / Trade-offs
Exclusion Angle	Restricts NGSO operation within a predefined angular region relative to GSO links to avoid in-line interference	Satellite positions, NGSO–GSO geometry, line-of-sight angles	Network planning and operational constraints (geometric restrictions)	Simple and effective in reducing EPFD	Reduces NGSO coverage; creates exclusion zones dependent on latitude
PC	Dynamically adjusts transmit power to satisfy interference constraints	Distance to GSO receivers, interference thresholds (e.g., EPFD), channel conditions	Real-time or semi-static control algorithms and optimization methods	Flexible; maintains service while mitigating interference	May reduce system capacity; requires continuous monitoring
Beamforming	Adapts antenna radiation pattern (e.g., null steering) to suppress interference	Receiver direction, channel state, spatial geometry	Digital signal processing with phased-array antennas	High spectral efficiency; avoids shutting down links	High computational and hardware complexity
Beam-tilting	Adjusts beam direction to increase angular separation between NGSO and GSO systems	NGSO–GSO geometry, link directions	Electronic control of antenna pointing direction	Simple extension of beamforming; no need to modify constellation	May degrade coverage or service quality in some regions
Movable Antennas	Physically repositions antenna elements to optimize radiation pattern	User distribution, interference environment, channel parameters	Mechanical control combined with optimization algorithms (e.g., simulated annealing)	High flexibility; improves SINR and interference control	High mechanical and computational complexity
RL	Learns optimal interference mitigation policies via interaction with the environment	System state (interference, traffic, channel), reward function	Machine learning algorithms (e.g., PPO, multi-armed bandits)	Adaptive and suitable for dynamic environments	High training and computational cost
Joint Techniques	Combines multiple techniques (e.g., PC + beam-tilting, BS + sidelobe level, PC + BS, etc.)	Depends on combined methods (geometry, channel, interference, etc.)	Integrated multi-parameter optimization and control	Superior overall performance; better compliance with ITU constraints	Increased system complexity and implementation cost

traffic demands. Simulation results demonstrate that this algorithm increase the overall system throughput, showing its effective interference coordination in the coexistence between satellite systems.

2.2 Cooperative Interference Mitigation Strategies

A cooperative strategy is defined as an approach in which NGSO and GSO systems share operational data. By synchronizing their operations, where the GSO system acts as the primary spectrum user and the NGSO system as a secondary user; the NGSO satellites can operate more efficiently, thereby improving the overall quality of service. One application of cooperative strategies arises in the context of satellite operators managing multi-orbit systems, wherein the constituent systems possess complete mutual access to each other's information. Recent research on cooperative strategies involves the following techniques:

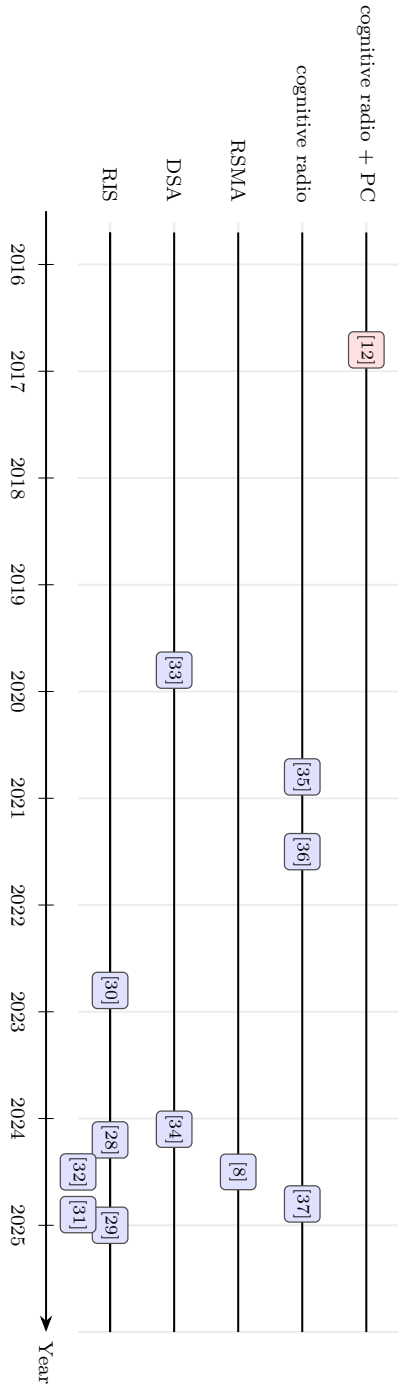

Figure 2.4 – Timeline of publications on cooperative mitigation techniques.

reconfigurable intelligent surfaces (RIS), dynamic spectrum access (DSA) and cognitive radio (CR). The latest applications of these approaches are discussed in the following subsections. For a more explicit overview, Fig. 2.4 presents a graphical timeline of the publications on each cooperative techniques addressed in this section, in which and as mentioned before, the references in blue are the ones related to a single interference mitigation technique and, in red, the ones with a joint approach.

2.2.1 Reconfigurable Intelligent Surfaces

RIS technology consists of programmable passive surfaces capable of directing reflected signals toward desired directions, thereby enhancing signal quality and extending coverage [29]. Fig. 2.5 illustrates the use of RIS in satellite systems.

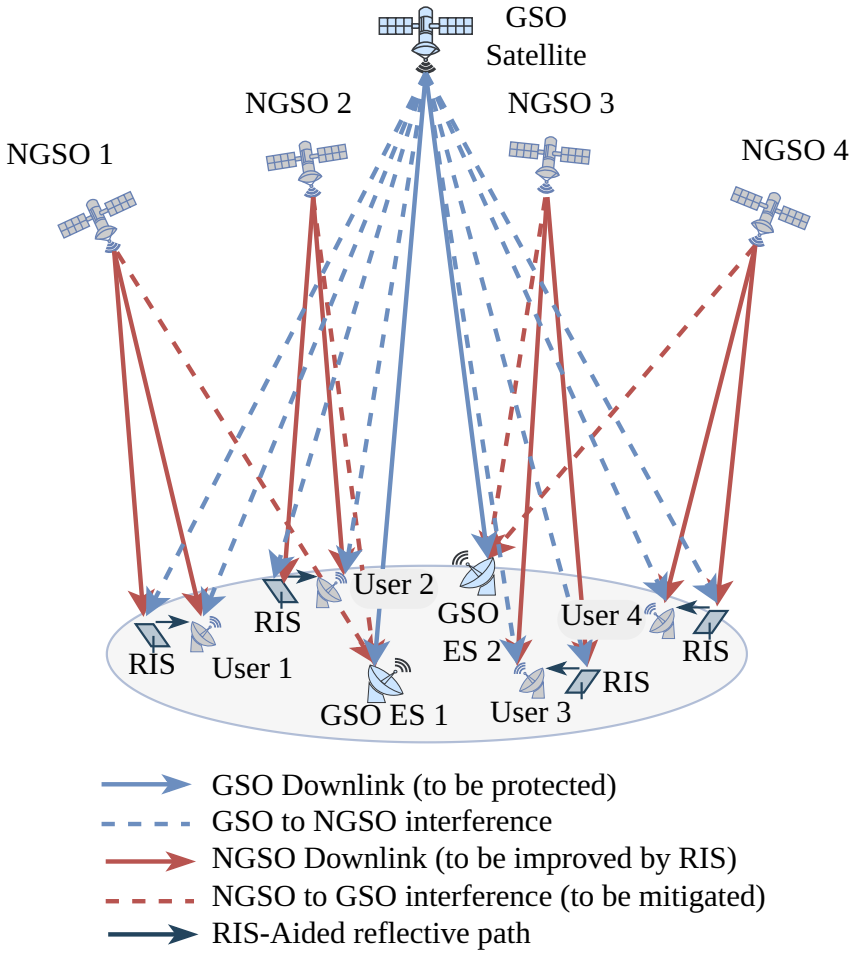

Figure 2.5 – GSO-NGSO spectrum-sharing with RIS-aided reflecting paths.

One approach to address NGSO–GSO interference involves integrating RIS into satellite communication systems, as discussed in [29]. In the framework proposed by the authors, multiple NGSO satellites cooperate with ground-deployed RIS units to implement joint multi-satellite multi-RIS beamforming. The objective is to maximize the minimum SINR for NGSO users while satisfying stringent NGSO–GSO interference mitigation requirements. Simulation results demonstrate that this RIS-assisted strategy effectively reduces NGSO–GSO interference, ensuring compliance with ITU regulations, and significantly enhancing the performance of NGSO satellite communications.

The authors in [30] design cooperative beamforming under a non-coherent cell-free multiple-input multiple-output (MIMO) paradigm, combining adaptive and maximum ratio precoding with statistical and two-timescale channel state information. They develop several algorithms, including an alternating optimization based method, a power allocation

algorithm, and a two-stage adaptive and maximum ratio precoding established design to jointly augment active and passive beamforming. Numerical results demonstrate significant gains in signal quality, fairness, and interference suppression, highlighting the effectiveness of multi-satellite cooperation and RIS integration between the sixth generation (6G) of mobile networks and satellite communication systems.

Merging deep reinforcement learning (DRL) and RIS, the articles [31] and [32] proposes a DRL framework for secure multiuser multiple-input single-output (MISO) satellite downlink systems assisted by hybrid RIS, which combine active and passive reflective elements. The goal is to maximize the system secrecy rate by jointly optimizing satellite and RIS beamforming under imperfect and outdated channel state information and practical power constraints. The authors employ a deep deterministic policy gradient algorithm to handle the non-convex and high-dimensional optimization problem, enabling adaptive beamforming in dynamic satellite environments. Simulation results demonstrate that the proposed hybrid-RIS design significantly outperforms conventional passive RIS in terms of secrecy rate and robustness, achieving up to 36% improvement while maintaining lower power consumption.

In another approach, the article [33] proposes a new framework to improve the energy and spectral efficiency of NGSO satellite networks using RIS and non-orthogonal multiple access (NOMA). The study addresses challenges such as high power consumption, spectrum congestion, and weak satellite-to-ground links—particularly for mobile users with low-gain antennas. It formulates a non-convex optimization problem that jointly optimizes the satellite's transmit power and RIS passive beamforming under imperfect successive interference cancellation conditions. The problem is solved through an alternating optimization approach, combining Lagrangian dual methods and semi-definite programming. Simulation results demonstrate that the proposed RIS-NOMA framework improves energy efficiency by 21.47% and 54.9% compared to benchmark and conventional NOMA models, respectively, while converging rapidly with low computational complexity.

2.2.2 Dynamic Spectrum Access

DSA is a flexible and adaptative approach to spectrum management that allows systems to use frequency bands based on real-time availability rather than being restricted to fixed allocations [34].

The authors in [35] investigates a DSA framework where secondary NGSO satellites opportunistically reuse frequency bands allocated to primary GSO satellites. The model incorporates the time-varying characteristics of the satellite network, including the moviment of NGSO satellites and Earth's rotation, which generate dynamic interference patterns. GSO downlink transmissions are assumed to employ an orthogonal multiple access scheme. A key finding is that NGSO transmissions do not interfere with GSO users, provided that each

NGSO satellite reuses only the frequency bands unassigned to GSO users within its coverage footprint. Simulation results indicate that the DSA approach achieves superior throughput for NGSO satellites compared to conventional orthogonal multiple access, particularly as GSO user density increases. Furthermore, average NGSO throughput decreases with increasing satellite altitude, since larger coverage areas encompass more GSO users, reducing the number of frequency bands available for reuse.

2.2.3 Other Advanced Mitigation Techniques

On rate-splitting multiple access (RSMA), a message is shared between GSO and NGSO satellites to allow the coexistence of system at the same frequency band. By sharing information, the GSO users can mitigate in-line interference from the NGSO satellites using successive interference cancellation, as in [36].

Under shared spectrum scenarios, conventional interference management often fails to balance throughput and fairness under heterogeneous user traffic demands. RSMA enables signal decomposition into common and private components, providing flexible interference mitigation. The authors in [36] formulate a throughput maximization problem under traffic-awareness constraints, ensuring that resource allocation aligns with varying user demands. The traffic-aware design ensures that high-demand users receive sufficient resources without severely degrading service to others. The study demonstrates that RSMA combined with traffic-aware optimization is a promising solution for interference management and spectrum efficiency in GSO–NGSO coexisting networks.

Cognitive radio technology has been used to share spectrum resources among terrestrial systems due to spectrum scarcity. Now it is being applied to space operations in a novel approach. In satellite operations, cognitive radio is effective for supporting the co-existence of two or more satellite systems, in which the GSO satellite is the primary user of the frequency band and the NGSO satellites are the secondary users [37].

In [37], a cooperative framework is introduced that jointly optimizes power allocation and inter-satellite coordination. GSO satellites are treated as primary users, maintaining required SINR thresholds, while NGSO satellites, as secondary users, cooperatively adjust power and beam assignments to maximize throughput without degrading GSO service. The problem is formulated as a mixed-integer nonlinear programming model, which is then decomposed into three lower-complexity sub-problems: beam and user allocation, beam PC, and time-proportional allocation. Results indicate that this cooperative spectrum sharing approach significantly improves NGSO throughput and system capacity relative to conventional beam-hopping and cooperative beam-hopping methods, demonstrating the effectiveness of integrating inter-satellite cooperation with optimized power allocation for future congested-spectrum scenarios.

To enable effective spectrum sharing without silencing NGSO transmissions, the authors in [38] propose a cooperative spectrum sharing scheme. The design incorporates queue backlog and fairness metrics via Lyapunov drift theory to maintain system stability and reduce service latency. Unlike exclusion zone or CR approaches that silence NGSO transmissions near GSO beams, this method allows NGSO users to remain active, avoiding service blackouts. Simulations show faster convergence, improved handling of high traffic loads, and higher NGSO data rates while ensuring GSO protection.

Finally, [39] studies how to maximize spectral efficiency in cognitive radio-based GSO–NGSO coexisting satellite networks, where both systems share spectrum but interfere with each other's ground users. To address this challenge, the authors develop an Earth rotation-aware non-stationary communication distance model that captures the variation in distances between NGSO satellites and ground terminals over time. They then formulate a power optimization problem that jointly considers interference thresholds, transmission requirements, and the movement of NGSO satellites. Results demonstrate that the proposed scheme significantly improves spectral efficiency compared with benchmark fixed-power strategies, while ensuring that the GSO system (as the primary user) is protected from harmful interference. The authors highlight that NGSO transmissions are more efficient when satellites are closer to users, and spectral efficiency improves when spectrum access is coordinated around these periods.

2.2.4 Joint Techniques

Besides being used in non-cooperative strategies, PC can also be applied in cooperative strategies. As mentioned in Section 2.1.2, document [13] brings power control in both scenarios.

In the case of cooperative strategies, article [13] gives an overview of cognitive range-based PC (C-PC) and traffic-aware PC (TA-PC), as also developed in [36]. C-PC considers interference thresholds at GSO terminals, while TA-PC adapts transmission power to time-varying traffic demands, reducing unnecessary interference and power consumption.

Simulations show that TA-PC improves overall performance, but C-PC remains the most effective method to maintain interference below harmful levels. The combination of cognitive PC and optimized earth terminal placement offers a robust framework for sustainable NGSO–GSO coexistence under shared Ka-band spectrum.

2.3 GSO-NGSO Interference Detection

For interference detection, conventional techniques such as energy detectors have been widely employed, as mentioned in [40]. However, under complex NGSO-to-GSO coexistence scenarios, this method often fails to identify weak or hidden interference. This limitation

Table 2.2 – Summary of cooperative interference mitigation techniques

Technique	Working Principle	Required Information	Implementation	Advantages	Limitations / Trade-offs
RIS	Programmable passive surfaces reflect and steer signals to enhance desired links and suppress interference via cooperative beamforming	Channel state information (CSI), satellite positions, RIS configuration, user locations	Joint satellite–RIS beamforming optimization and passive phase control	Significant SINR improvement; enhanced coverage and interference suppression	Requires accurate CSI; high optimization complexity; deployment of RIS infrastructure
DSA	NGSO satellites opportunistically reuse spectrum not occupied by GSO users based on real-time availability	Spectrum occupancy, user distribution, satellite coverage, time-varying network conditions	Dynamic frequency allocation and spectrum sensing mechanisms	Efficient spectrum utilization; increased NGSO throughput	Requires reliable sensing; performance depends on GSO user density and dynamics
RSMA	Splits messages into common and private parts, enabling interference mitigation via successive interference cancellation at receivers	Channel conditions, traffic demand, interference levels	Signal processing and resource allocation with joint encoding/decoding strategies	Flexible interference management; improved fairness and throughput	Increased receiver complexity; requires coordination between systems
Cognitive Radio	NGSO operates as secondary user, adapting transmission based on sensing and protection of primary GSO system	Spectrum sensing data, interference thresholds, channel conditions	Adaptive power control, beam allocation, and spectrum access strategies	Enables coexistence without strict exclusion zones; improves spectral efficiency	Challenging spectrum sensing; risk of interference if detection is inaccurate
Joint Techniques	Combines multiple cooperative methods (e.g., Cognitive Radio + PC) for enhanced interference mitigation	Integrated system information (CSI, traffic, geometry, interference constraints)	Cross-layer optimization and coordinated multi-system resource management	Superior overall performance; improved spectral efficiency and coexistence	High implementation complexity; requires tight synchronization and data exchange

has motivated the adoption of machine learning and artificial intelligence (AI) techniques as more robust alternatives for interference detection between NGSO and GSO systems.

Studies explored the use of deep learning models for NGSO-to-GSO interference detection. In [41], an autoencoder (AE) neural network is proposed to detect interference in both time- and frequency-domain signals. The AE is prepared considering datasets for training and testing in a simulated environment and evaluated as an anomaly detection task. The model is constructed taking into account the mean average error (MAE) as the loss function and a threshold is first established. Then, the inputs are classified as anomalous if the reconstruction error is higher than the standard deviation from the training sets. Simulations showed superior performance in the time-domain representation, achieving up to 100% detection accuracy, while in the frequency-domain results reached 99.9%.

Building on this foundation, the authors in [40] investigated more advanced generative AI models to improve detection capabilities, including a variational autoencoder (VAE) and a transformer-based interference detector (TrID). The approaches learned compact representations of expected GSO signals, with detection based on reconstruction error. Comparative

evaluations demonstrated that VAE and TrID outperformed benchmark architectures, including AE, convolutional autoencoder, and long short-term memory autoencoder, as well as traditional energy detector (ED). The TrID model, in particular, consistently outperformed all other models and the traditional ED approach. TrID demonstrated greater robustness across various scenarios, including different GSO modulation schemes, bandwidth overlaps, NGSO off-axis angles, and interference power levels. VAE also performed well and is effective at minimizing false alarms, but its results are less consistent compared to TrID in scenarios with reduced bandwidth overlap, making TrID a more reliable choice for diverse conditions.

In [42] it is proposed the use of unsupervised deep learning, specifically convolutional autoencoders (CAEs), to detect interference from NGSO satellites—mainly LEO systems—affecting GSO ground stations. The authors design two models: CAE1D, which processes signal amplitude as one-dimensional data, and CAE2D, which processes in-phase/quadrature (I/Q) samples as two-dimensional data. They evaluate both single-model and multi-model training approaches and compare the results against traditional ED methods. Simulations using realistic satellite parameters show that deep learning models, especially CAE1D trained under the multi-model approach, outperform conventional techniques by up to 11% in detection probability. The findings demonstrate that CAEs can effectively enhance interference detection in complex, dynamic satellite environments, offering a promising solution for future interference management in mixed GSO–NGSO systems.

The authors in [43] investigates how different dataset representations affect the performance of convolutional neural networks (CNNs) for detecting and classifying radio-frequency interference directly onboard GSO satellites. The study considers interference from NGSO systems sharing the same spectrum and evaluates CNN performance using various fast Fourier transform (FFT) representations—complex and magnitude values of full dimension and reduced dimension FFT. Simulation results show that using the magnitude of the reduced dimension FFT achieves the highest accuracy (up to 100% in some cases) for interference detection and localization within the spectrum, outperforming other data types. The results highlight that selecting an appropriate data representation significantly enhances CNN-based interference detection efficiency while reducing computational complexity, making it suitable for real-time on-board satellite applications.

2.4 Challenges and Future Directions

The key challenges concerning interference between the NGSO and GSO satellite systems are as follows:

- The nonalignment of ITU-R frameworks with the rapid technological advancements in satellite communications.
- There is no universally accepted methodology for accurately modeling an NGSO system.

- Although large-scale NGSO constellations have only recently begun widespread deployment, the ITU-R frameworks governing NGSO operations were largely established more than two decades ago and may no longer reflect current realities.
- While existing regulations define EPFD limits to protect GSO satellites from individual NGSO systems, they do not establish aggregate EPFD limits to safeguard GSO services against simultaneous interference from multiple NGSO systems.

Despite these limitations, NGSO systems bring a wide range of opportunities, and several future research directions can be envisioned, such as:

- **Integration of satellite and terrestrial networks**: it will enable standard consumer devices, such as smartphones and internet of things (IoT) terminals, to establish direct communication with satellites without the need for dedicated ground infrastructure. This paradigm is supported by advancements in NGSO constellations, adaptive beamforming, and 3rd Generation Partnership Project (3GPP) standardization (*e.g.*, Release 17 for non-terrestrial networks), which ensure interoperability between satellite and terrestrial mobile networks. This integration has the potential to provide truly global coverage for applications including emergency messaging, IoT connectivity, and, in the future, broadband services. Ongoing collaborations between satellite operators and mobile network providers further reinforce the pivotal milestone toward the seamless convergence of satellite and terrestrial communication ecosystems.
- **New frequency bands for NGSO operations**: the most used frequency band for broadband high data rate are Ku band, 10/14 GHz, and Ka band, 20/30 GHz. Now, higher frequency bands, like Q/V bands, 40/50 GHz, and E band, 70/80 GHz, started to be considered as broadband, especially due to the large number of NGSO satellite systems being deployed in the recent years and the fact that orbit and spectrum are limited resources. The running for new NGSO frequency bands is a continuous reality considering that the NGSO systems are being seen as the future of satellite communications due to the congestion of the GSO orbital arc. This also brings some challenges since it is necessary to share spectrum with other services, not only satellite but also terrestrial, and sharing and compatibility studies are required.
- **Space sustainability for future generations**: With the rapid growth of satellites, especially large NGSO constellations, concerns about orbital congestion, collision risks, and space debris have intensified. Ensuring sustainability involves adopting measures such as debris mitigation guidelines, end-of-life disposal, active debris removal, and improved space traffic management. It also requires international cooperation, regulatory frameworks, and industry best practices to balance innovation with the preservation of the orbital environment, making sustainability a cornerstone for the future of space activities.

2.5 Conclusions

This chapter has reviewed recent articles addressing NGSO–GSO coexistence, providing a comprehensive analysis of non-cooperative and cooperative interference mitigation strategies, as well as emerging approaches for interference detection leveraging machine learning and GenAI. By consolidating current advances and open challenges, the chapter underscores the importance of continued research in NGSO–GSO coexistence, aiming to ensure resilient, efficient, and globally scalable satellite communications.

3 Joint Power Control and Beam Steering for NGSO-to-GSO Interference Mitigation in Ku Band

Considering the analysis of the mitigation techniques presented in Chapter 2, in this chapter we jointly apply PC and BS techniques to NGSO satellites within a defined angular mitigation zone and an arc-based system model. The approach in this chapter avoids tight synchronization between system elements, relying only on geometric parameters known in advance by both GSO and NGSO systems.

3.1 System Model

The adopted system model considers a GSO satellite positioned at an altitude of h_{GSO} relative to the Earth surface, providing coverage over an arc on the Earth's surface with length $\ell_{\text{c}} = 2\Delta\alpha R_{\text{e}}$, in which $R_{\text{e}} = 6378$ km is the Earth's radius and $\Delta\alpha$ is the angular span of the arc with respect to the Earth's center. The parameter $\Delta\alpha$ represents the angular extent of the GSO satellite footprint with respect to the center of the Earth. Each point along the arc represents a GSO earth station whose antenna main lobe is directed towards the GSO satellite. In this scenario, a constellation of N_{s} NGSO satellites, in circular orbits at an altitude h_{NGSO} above the Earth's surface, generates interference toward the GSO ground stations. The NGSO satellites are assumed to employ nadir-pointing antennas, with their main lobes directed toward the Earth's center. The system model is illustrated in Fig. 3.1.

Assuming that the GSO satellite antenna has a main lobe with an angular width of $2\Delta\beta$, the corresponding earth-centered coverage footprint subtends an angular width given by

$$\Delta\alpha = \arcsin\left[\left(\frac{R_{\text{e}} + h_{\text{GSO}}}{R_{\text{e}}}\right)\sin(\Delta\beta)\right] - \Delta\beta. \tag{3.1}$$

In turn, the positions of the N_{s} NGSO satellites are defined as

$$\mathbf{s}_n = h_{\text{NGSO}}[\cos(n\Delta\theta + \pi/2), \sin(n\Delta\theta + \pi/2)]^T, \tag{3.2}$$

where $[\,\cdot\,]^T$ denotes the transpose operator, $n \in \{0, 1, \ldots, N_{\text{s}} - 1\}$, and $\Delta\theta = 2\pi/N_{\text{s}}$. This configuration forms a circular network with a satellite density of $\rho_{\text{s}} = \frac{N_{\text{s}}}{2\pi}$ satellites per radian. Considering a coordinate system referenced at the Earth center, the main beam direction vector of the n-th NGSO satellite is given by $\mathbf{b}_n = -\mathbf{s}_n/h_{\text{NGSO}}$. The radiation pattern of the

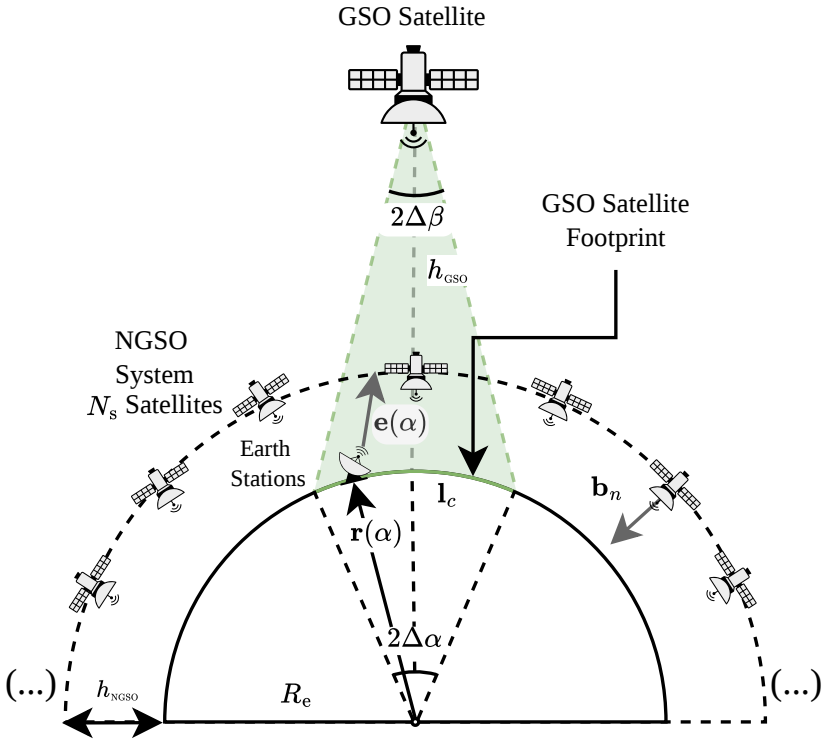

Figure 3.1 – System model.

NGSO antennas is modeled according to [44] as[1]

$$G_{\text{tx}}(\varphi) = \bar{G}_{\text{tx}} \left| 2\frac{J_1[\pi\delta_{\text{tx}}\sin(\varphi)]}{\pi\delta_{\text{tx}}\sin(\varphi)} \prod_{k=1}^{K-1} \frac{1 - \left[\frac{\delta_{\text{tx}}\sin(\varphi)}{\sigma u_k}\right]^2}{1 - \left[\frac{\delta_{\text{tx}}\sin(\varphi)}{\mu_k}\right]^2} \right|^2, \tag{3.3}$$

where $\bar{G}_{\text{tx}}$ is the maximum gain, φ is the observation angle relative to the antenna's boresight (main lobe axis), K is a number controlling the degree of uniformity of the sidelobes, and $J_1(\cdot)$ is the first-order Bessel function of the first kind. The parameter δ_{tx} represents the antenna aperture size in wavelengths. The terms $u_k = \sqrt{A^2 + (k - 1/2)^2}$ and $A = \text{arcCosh}\left(10^{S/10}\right)/\pi$ characterize the sidelobe structure, where S is the sidelobe level in decibels (dB). The parameter μ_k is the k-th zero of $J_1(\cdot)$, and $\sigma = \mu_K/u_K$ is the dilatation factor.

In turn, the positions of the GSO ground stations are expressed as $\mathbf{r}(\alpha) = R_e[\cos(\alpha + \pi/2), \sin(\alpha + \pi/2)]$, in which $\alpha \in [-\Delta\alpha, \Delta\alpha]$. The main beam vector of the ground stations antennas is defined as $\mathbf{e}(\alpha) = [\mathbf{g} - \mathbf{r}(\alpha)]/\|\mathbf{g} - \mathbf{r}(\alpha)\|$, in which $\mathbf{g}$ is the position vector of the GSO satellite and $\|\cdot\|$ denotes the Euclidean norm. Radio Regulations Article 22 determines that, for interference simulations between GSO and NGSO systems in Ku band (10-14 GHz),

[1] Initially, Recommendation ITU-R S.1528-0 [45, item 1.4] was adopted to model the NGSO satellite antenna pattern. However, further analysis—supported by ESA's working document [46] submitted to the May 2025 ITU-R WP4A meeting—revealed inconsistencies in the sidelobe characterization. One reference cited in the Recommendation is [44], which presents a pattern with minor differences but improved sidelobe control. Therefore, the antenna model based on [44] was adopted for the simulations in this study.

the antenna for the GSO earth station should comply with the antenna pattern listed in Recommendation ITU-R S.1428 [47]. Based on this recommendation, the radiation pattern depends on the effective antenna dimension (in wavelengths), denoted as δ_{rx}. For the case of the simulations of this study, an antenna of 60 cm was chosen, which represents a $\delta_{\text{rx}} = 21.4$. Fig. 3.2 illustrates the normalized radiation patterns of the antennas considered in the system model, in which the NGSO satellite antenna is designed with $K = 4$ and $\delta_{\text{tx}} = 10.7$.

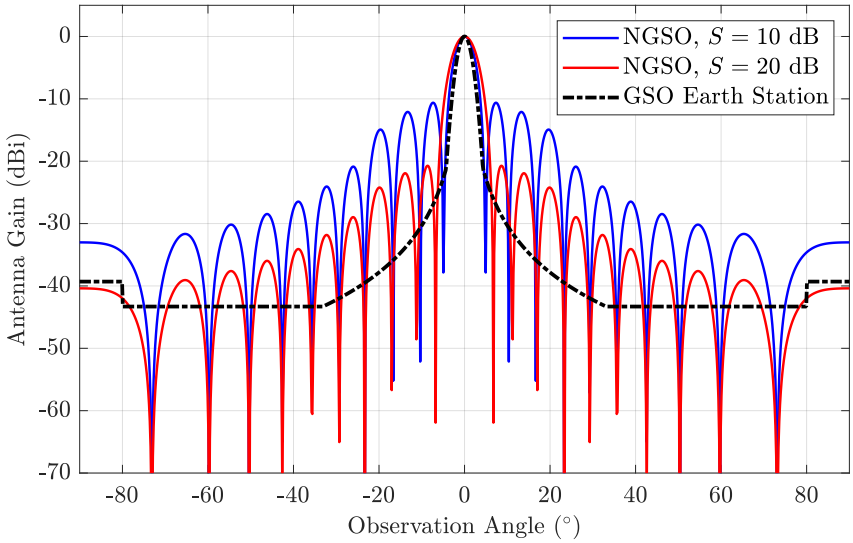

Figure 3.2 – Normalized antenna radiation patterns of GSO earth station and NGSO satellites as a function of observation angle. NGSO satellite antennas are evaluated with different values of the sidelobe level S.

3.1.1 Interference Analysis

The ITU-R regulations governing interference between NGSO and GSO systems in the Ku band are based on the EPFD, which quantifies the aggregate power flux density emitted by the interfering system toward the victim receiver. In this work, we evaluate the EPFD in the downlink, where the victim receiver is the GSO ground station, and the interfering source is the NGSO satellite network. The EPFD at a ground station located at an arbitrary angle α within the GSO coverage footprint is given by [48]

$$\text{EPFD}(\alpha) = \sum_{n \in \mathcal{S}_{\text{v}}(\alpha)} P_{\text{t}} \frac{G_{\text{tx}}(\varphi_n)}{4\pi d_n^2(\alpha)} \frac{G_{\text{rx}}(\varphi'_n)}{\bar{G}_{\text{rx}}}, \tag{3.4}$$

in which $\mathcal{S}_{\text{v}}(\alpha)$ is the set of visible NGSO satellites at position α, P_{t} is the RF power at the input NGSO antenna of the transmit station in the reference bandwidth and $\bar{G}_{\text{rx}}$ is earth station maximum antenna gain. The term $d_n(\alpha)$ is the distance between the earth station and the n-th visible satellite, computed by $d_n(\alpha) = \|\mathbf{s}_n - \mathbf{r}(\alpha)\|$. The angle φ' is the angular separation between the boresight vector $\mathbf{e}(\alpha)$ and the vector $\mathbf{x}_n = \mathbf{s}_n - \mathbf{r}(\alpha)$. In turn, the

angular separation φ_n is defined as the angle between boresight vector $\mathbf{b}_n$ and $-\mathbf{x}_n$. The set of satellites visible for a given position α is determined as

$$\mathcal{S}_{\mathrm{v}}(\alpha) = \{n \in \{0,1,\cdots,N_{\mathrm{s}}-1\} | \langle \mathbf{r}(\alpha), \mathbf{x}_n \rangle > 0\}, \tag{3.5}$$

in which $\langle \cdot, \cdot \rangle$ represents the dot product. According to (3.5), a satellite is considered visible if it is located above the local horizon of the ground station at position $\mathbf{r}(\alpha)$.

3.1.2 Interference Mitigation Techniques

Article 22 of the ITU-R Radio Regulations defines that, for operations in the Ku band, the EPFD must not exceed -160 dB(W/m^2) over a reference bandwidth of 40 kHz to ensure adequate protection and proper operation of terrestrial GSO systems. In this context, we implement interference mitigation techniques based on an angular mitigation zone defined with respect to the Earth's center, characterized by an angular width $\Delta\vartheta$. To ensure protection of the ground stations located at the extreme points of the coverage footprint, the mitigation region must satisfy $\Delta\vartheta \geq \Delta\alpha$. NGSO satellites located within this exclusion region can jointly employ two complementary interference mitigation techniques, namely: PC and BS. In the PC approach, satellites reduce their transmit power by a predefined factor when operating inside the angular mitigation zone, thereby decreasing the power flux density incident on the Earth's surface. In the BS approach, electronically steerable phased array antennas are used to redirect the main beam away from the mitigation region, thus reducing interference toward GSO ground stations. It is assumed that each NGSO satellite operates with a single beam. Furthermore, during the BS, NGSO satellites located outside the mitigation zone are responsible for providing coverage to areas not served by the satellites within the mitigation zone. Fig. 3.3 illustrates these interference mitigation techniques. It is important to note that this approach does not require tight synchronization between system elements, as it relies solely on geometric parameters that can be determined a priori by both the GSO and NGSO systems.

For a given position $\mathbf{r}(\alpha)$, let $\mathcal{S}_{\mathrm{a}}(\alpha) \subset \mathcal{S}_{\mathrm{v}}(\alpha)$ denote the subset of visible satellites that are located within the angular region where interference mitigation is applied. In this case, the EPFD considering the mitigation techniques can be expressed as

$$\mathrm{EPFD}(\alpha) = \sum_{n \in \mathcal{S}_{\mathrm{v}}(\alpha) \setminus \mathcal{S}_{\mathrm{a}}(\alpha)} P_{\mathrm{t}} \frac{G_{\mathrm{tx}}(\varphi_n)}{4\pi d_n^2(\alpha)} \frac{G_{\mathrm{rx}}(\varphi_n')}{\bar{G}_{\mathrm{rx}}} + \sum_{m \in \mathcal{S}_{\mathrm{a}}(\alpha)} (\kappa P_{\mathrm{t}}) \frac{G_{\mathrm{tx}}(\varphi_m + \bar{\varphi})}{4\pi d_m^2(\alpha)} \frac{G_{\mathrm{rx}}(\varphi_m')}{\bar{G}_{\mathrm{rx}}}, \tag{3.6}$$

where $\kappa \leq 1$ represents the power reduction factor and $\bar{\varphi}$ is the BS angle. When $\kappa = 1$ or 0 dB, (3.6) corresponds to the case where only the BS technique is applied. Conversely, when $\bar{\varphi} = 0$, the expression reduces to the scenario where only PC is applied. The limiting case of PC occurs when $\kappa = 0$, meaning that NGSO satellites within the mitigation region are

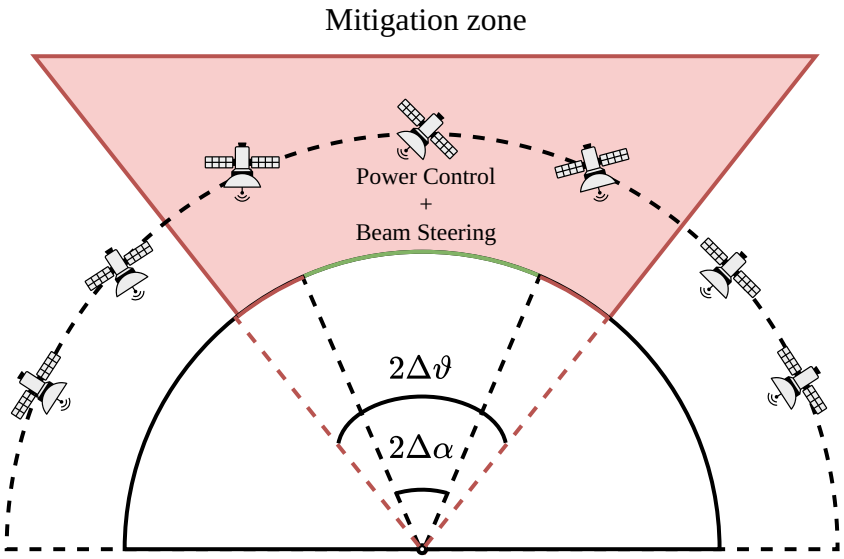

Figure 3.3 – Illustration of the region and interference mitigation techniques.

completely turned off. The effectiveness of the BS technique depends considerably on the sidelobe level S of the NGSO satellite antennas, since this factor characterizes the strength of the sidelobes.

3.2 Numerical Results

The simulations[2] are conducted at a frequency of 10.7 GHz, corresponding to a wavelength of $\lambda = 2.8$ cm. The GSO satellite is positioned at an altitude of $h_{\text{GSO}} = 35786$ km and employs an antenna with an effective beamwidth of $2\Delta\beta = 5°$. Using (3.1), the satellite's footprint spans an angular width of $\Delta\alpha = 14.25°$ relative to the Earth's center. The ground station antennas have a normalized aperture size of $\delta_{\text{rx}} = 21.4$, which, according to Recommendation ITU-R S.1428 , corresponds to a maximum gain of $\bar{G}_{\text{rx}} = 34.3$ dBi. In [26], the NGSO satellites EIRP is –3.4 dBW in 40 kHz, in compliance with the ITU regulations reference bandwidth $B_{\text{w;ref}}$ for Ku band. The NGSO satellites are equipped with antennas featuring a maximum gain of 34 dBi, $K = 4$, a normalized aperture size of $\delta_{\text{tx}} = 10.7$ wavelengths and an orbital angular separation in the plane of $2\pi/N_s$. Taking these parameters into account, P_t is –37.4 dBW in 40 kHz. The simulation parameters are summarized in Table 3.1 and cumulative distribution function (CDF) curves for the combined mitigation techniques are presented later to evaluate their joint performance.

Fig. 3.4 shows EPFD curves as a function of the footprint angular range (α), for different values of κ, $\bar{\varphi}$ and $\Delta\vartheta$, considering a NGSO system of 1,000 satellites, 263 NGSO satellites visible to the GSO footprint at 1,200 km of altitude, operating with an antenna of a sidelobe level $S = 15$ dB. The EPFD curve without the use of any mitigation techniques is included

[2] The code is available at: https://github.com/lucianarnf/kuepfd-main

Table 3.1 – Simulations parameters.

Parameter	Value
Frequency	10.7 GHz
Wavelength – λ	2.8 cm
Reference bandwidth – $B_{w;ref}$	40 kHz
GSO satellite altitude – h_{GSO}	35786 km
GSO satellite beamwidth – $2\Delta\beta$	5°
EIRP in the $B_{w;ref}$	−3.4 dBW
NGSO satellite max. antenna gain – $\bar{G}_{tx}$	34 dBi
RF power at the input of the NGSO antenna transmit station in the $B_{w;ref}$ – P_t	−37.4 dBW
Footprint angular width – $2\Delta\alpha$	14.25°
Degree of uniformity of the sidelobes – K	4
Normalized NGSO satellite antenna size – δ_{tx}	10.7
Normalized earth station antenna size – δ_{rx}	21.4

as a reference. In all curves, the highest EPFD values occur when there is an alignment between the main lobe of a GSO ground station and an NGSO satellite (i.e., $\alpha = 0$). Without any mitigation techniques, the NGSO operation generates a maximum EPFD at the surface of the Earth of almost −130 dB(W/m^2)/40kHz.

The results also show that applying only a PC (κ) of −10 dB or a BS ($\bar{\varphi}$) of 20º, the EPFD peak does not meet the −160 dB(W/m^2)/40kHz requested in ITU-R RR Article 22 for the Ku band, with EPFD peaks of approximately -140 dB(W/m^2)/40kHz and -150 dB(W/m^2)/40kHz, respectively. In turn, compliance with the ITU-R RR Article 22 is achieved when PC and BS are used together. Finally, it can be seen that it is possible to protect more of the coverage area of the GSO satellite by increasing $2\Delta\vartheta$. This occurs because increasing $\Delta\vartheta$ expands angular mitigation zone, thereby subjecting a larger portion of NGSO satellites to interference control. For $2\Delta\vartheta = 10°$, only a portion of the arc is protected under both PC and BS techniques. However, the arc is only completely protected if we apply a larger angular mitigation zone, with $\Delta\vartheta = 30°$.

Fig. 3.5 presents the maximum EPFD observed within the GSO satellite footprint as a function of the PC factor (κ), without the use of BS ($\bar{\varphi} = 0º$), for different altitudes h_{NGSO} and $2\Delta\vartheta$ values. In the simulations, we consider a sidelobe level of $S = 15$ dB for a system with 2,000 satellites. It is observed that lower-altitude NGSO satellites result in higher EPFD levels due to their proximity to the Earth's surface. In addition, the path loss over a distance of 1000 km is approximately 6 dB, which conducts to different results for identical parameter settings at varying altitudes. Furthermore, increasing $2\Delta\vartheta$ widens the angular mitigation zone, including a larger range of satellites in the interference reduction process. This leads to a decrease in the maximum EPFD across the GSO footprint. However, for a fixed mitigation angle $2\Delta\vartheta$, a reduction in the PC factor κ does not necessarily result in a

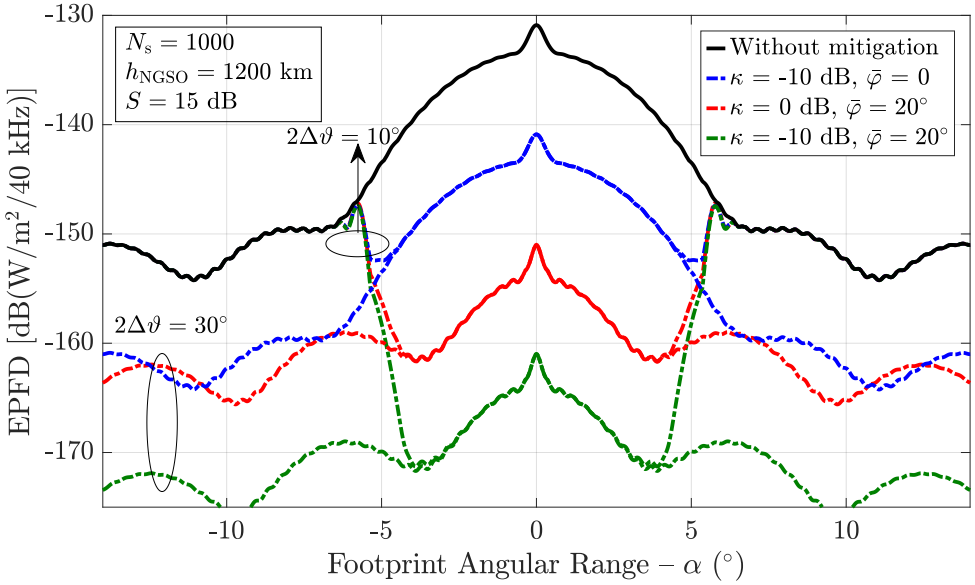

Figure 3.4 – EPFD curves along the angular range of the footprint considering $2\Delta\vartheta = 10°$ and $2\Delta\vartheta = 30°$ for different interference mitigation configurations.

proportional decrease in the maximum EPFD, as the power constraint is applied exclusively to satellites located within the defined mitigation region. As κ decreases, the system may reach a saturation regime in which the residual interference is primarily contributed by satellites outside the mitigation region, thereby making further reductions in κ ineffective in reducing the maximum EPFD.

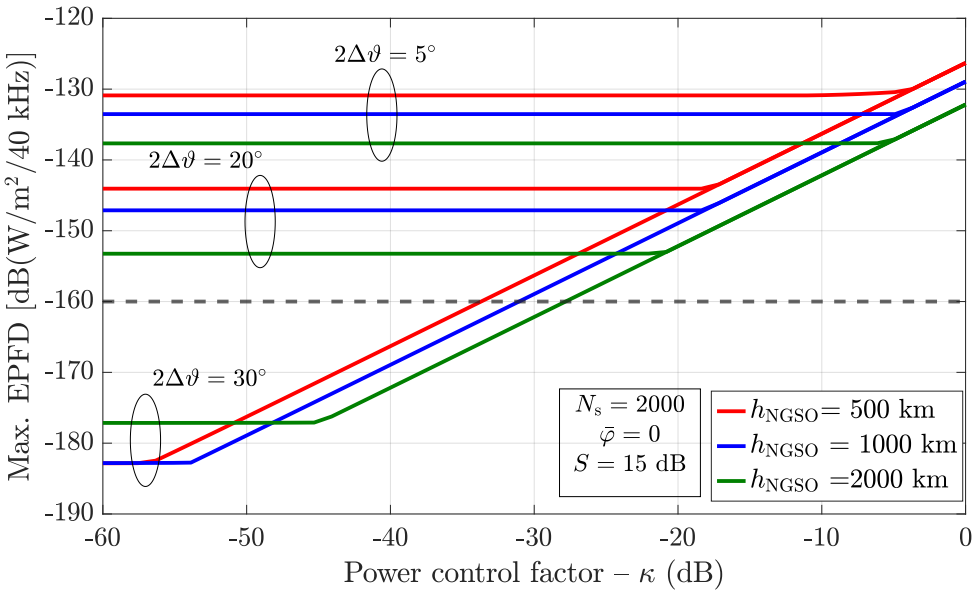

Figure 3.5 – Curves of maximum EPFD in the footprint arc as a function of the PC coefficient κ (dB), for different NGSO satellite altitudes and mitigation zone widths.

Fig. 3.6 presents the maximum EPFD as a function of the angle of BS ($\bar{\varphi}$), without the use of PC ($\kappa = 0$ dB), for different mitigation zone widths and different sidelobe (S) levels. We considered h_{NGSO} = 1,200 km and 2,000 satellites. First, it is important to emphasize that

the parameter S refers to the gain difference between the main lobe of the NGSO satellite antenna and its most significant secondary sidelobe. Thus, higher values of S implies lower sidelobe levels, which means that the antenna radiates less energy outside the main beam. Consequently, BS becomes more effective as S increases, since interference is generated due to weaker sidelobes level. For example, in the simulation, an S value of 30 dB implies that the main lobe is 30 dB stronger than the most prominent sidelobe. This explains the three distinct plateaus observed for different S values. Furthermore, as BS is applied to all NGSO satellites within the mitigation zone, the level of interference initially decreases. However, beyond a certain steering angle, further adjustments become ineffective because the sidelobes contribute negligibly, resulting in a constant EPFD value. Moreover, increasing the mitigation angle $2\Delta\vartheta$ leads to a larger number of satellites undergoing steering, which enhances the overall mitigation effect and results in a more noticeable EPFD reduction. The plateau effect is then observed at a later stage, irrespective of the number of satellites in the NGSO system.

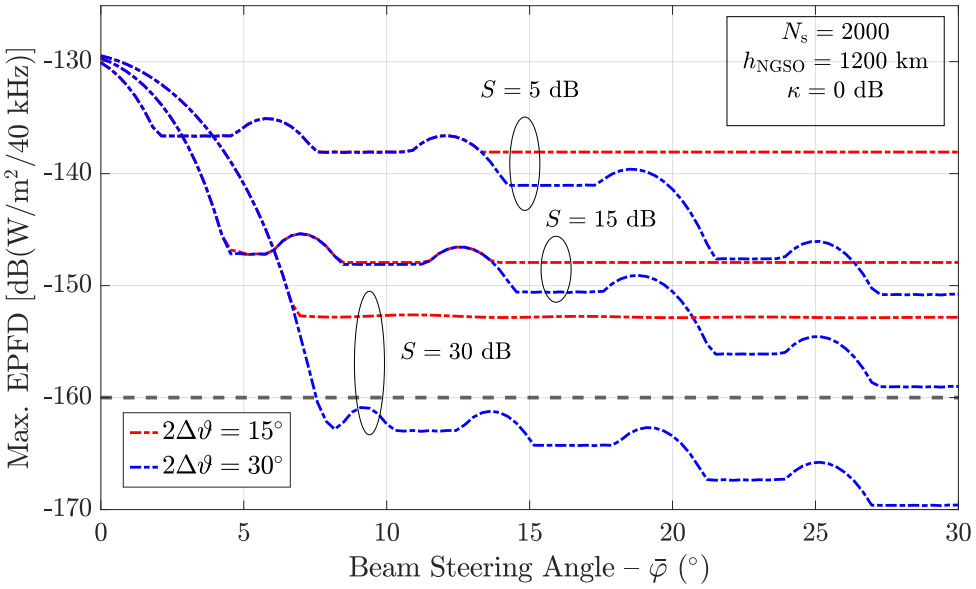

Figure 3.6 – Curves of maximum EPFD in the footprint arc as a function of the BS angle $\bar{\varphi}$, for different NGSO sidelobe levels and mitigation zone widths.

Fig. 3.7 presents EPFD CDF curves for different configurations of interference mitigation. Note that the CDF describes the probability of the EPFD being below a certain level. We considered in the simulations a NGSO system of 1000 satellites, $2\Delta\vartheta = 30^o$ and $S = 15$ dB. As benchmark, the EPFD CDF curve without the use of any mitigation technique is presented.

In this case, the EPFD almost certainly exceeds the ITU-R limits. For all scenarios, the joint use of PC and BS is effective to obtain EPFD levels below -160 dB(W/m^2)/40 kHz. It is important to note that as κ decreases from -10 dB to -30 dB, the probability of exceeding the EPFD level decreases. However, as κ becomes sufficiently small (*e.g.*, like -30 dB), the effect

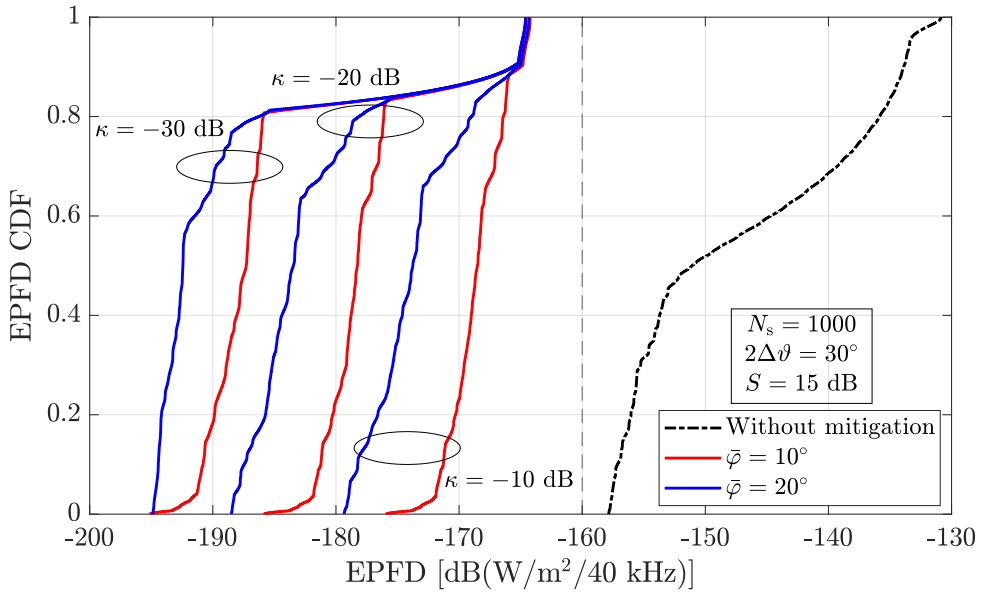

Figure 3.7 – EPFD CDF curves for different configurations of interference mitigation.

is similar to turn off the set of satellites in the $2\Delta\vartheta = 30^{o}$.

3.3 Conclusions

In this chapter, we presented a low-complexity approach to mitigate interference between NGSO and GSO satellite systems operating in the Ku band. By jointly applying PC and BS techniques, the proposed strategy effectively reduces the EPFD at GSO earth stations.

The impact of varying the angular width of the mitigation zone was analyzed, showing that a larger zone offers broader protection for the GSO coverage area. The proposed method contributes to the ongoing efforts to enable spectrum coexistence between NGSO and GSO systems, ensuring the safe and efficient use of satellite communications infrastructure.

4 Joint Power Control and Beam Steering to Mitigate NGSO-to-GSO Interference in Ku Band: A New Approach

To extend the analysis of Chapter 3 to a more realistic scenario, the GSO earth stations were distributed within the GSO footprint area, and NGSO satellites were arranged in multiple orbital planes using an algorithm proposed ITU-R Recommendation S.1503. Unlike the previous simplified configuration, the NGSO system is now spatially distributed over an area around the Earth, which significantly affected the results. Furthermore, the model is evaluated under large-scale NGSO systems deployments.

4.1 System Model

The system model in this chapter considers a GSO satellite that provides coverage to earth stations located within a given area on the Earth's surface, and a NGSO system whose orbital planes follow trajectories that intersect the GSO coverage footprint. The operation of the NGSO satellites network near the footprint causes interference to the links between ground stations and the GSO satellite. In this model, the GSO satellite is located at an altitude $h_{\mathrm{GSO}} = 35786$ km at the Equator's plane. Considering that the GSO antenna has a beamwidth denoted as $2\Delta\beta$ and that it points towards the center of the Earth (nadir), the footprint coverage has a circular outline and can be measured by an angle $2\Delta\alpha$ calculated by [27]

$$\Delta\alpha = \arcsin\left[\left(\frac{R_{\mathrm{e}} + h_{\mathrm{GSO}}}{R_{\mathrm{e}}}\right)\sin(\Delta\beta)\right] - \Delta\beta, \tag{4.1}$$

in which, $R_{\mathrm{e}} = 6378$ km is the Earth radius. The angle $\Delta\alpha$ mentioned in (4.1) is referenced to the Earth's center. Based on that, the footprint radius can be calculated by $R_{\mathrm{f}} = \tan(\Delta\alpha)R_{\mathrm{e}}$. This geometric model is illustrated in Fig. 4.1.

Within this GSO footprint, earth stations are homogeneously allocated. To determine the position of each earth station in longitude and latitude, it is necessary to calculate the footprint radius in terms of of geographic degrees, which is approximately 111 km. Considering that, the footprint streches over a region of approximately $r_{\mathrm{ang}} = [R_{\mathrm{f}}/(111 \times 10^3)] \times 1^\circ$. Thus, the positions of earth stations are distributed in a uniform grid with $P \times P$ positions, that extend in the range $[-r_{\mathrm{ang}}, r_{\mathrm{ang}}]$ in latitude and longitude. However, only the ones inside a circle of radius r_{ang} are considered in the simulations. In this configuration, a given ground station is indexed as (i,j), with $i,j \in \{1,\cdots,P\}$. Finally, the three-dimensional

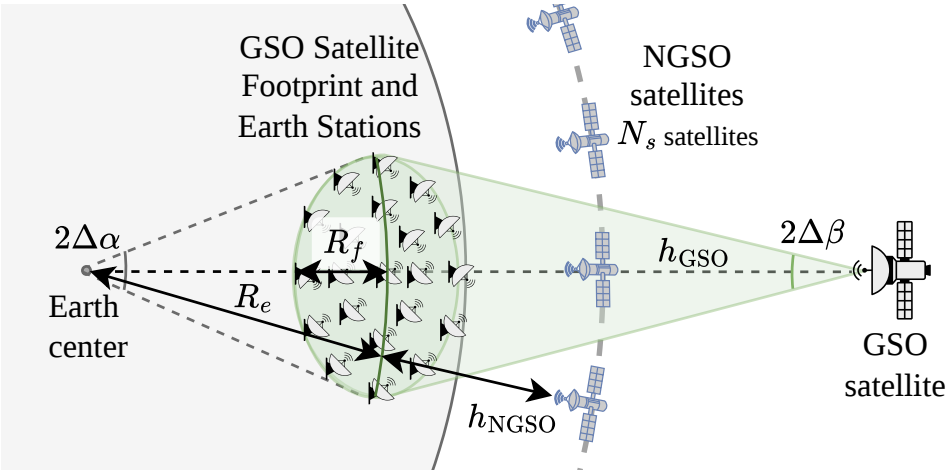

Figure 4.1 – System model illustration.

positions of ground stations are determined by converting latitude/longitude coordinates to spherical coordinates in the global (x,y,z)-coordinate system, denoted as $\mathbf{r}(i,j)$.

Besides the position of each GSO earth station, it is necessary to define the GSO earth stations antenna pattern. Recommendation ITU-R S.1428 [47] is adopted to characterize the radiation pattern of the GSO earth station antenna, as specified in Article 22 of the Radio Regulations for interference analyses between GSO and NGSO systems operating in the Ku band. According to this recommendation, the radiation pattern is a function of the effective antenna dimension, expressed in wavelengths and denoted by δ_{rx}. Furthermore, the GSO earth station antennas are pointing their main lobe toward the GSO satellite.

The next element of the system model is the NGSO system. It is assumed a network with N_{p} orbital planes, each containing N_{sp} satellites, adding a total of $N = N_{\text{p}} \times N_{\text{sp}}$ satellites. The position of a given satellite is defined based on the orbital geometry shown in Fig. 4.2. Considering an elliptical orbit, with perigee and apogee respectively written as R_{pe} and R_{ap}, the position of a NGSO satellite depends on the following angles: the longitude of the ascending node Ω, the inclination angle between the orbital plane and the equatorial plane i, the argument of perigee ω, and the true anomaly, representing the angle between the perigee and a specified point along the orbit, denoted as ν. In view of these parameters, the Cartesian position vector of each NGSO satellite can be determined using the algorithm described in Section D6.3.3 of Recommendation ITU-R S.1503 [9].

Initially, the position vector of the NGSO satellite is described in a coordinate system referenced to the orbital plane, denoted as (p,q)-coordinates. The procedure requires the computation of ω, Ω, and the mean anomaly M, which is related to Kepler's equation $M = E - e\sin(E)$, with e representing the eccentricity of the orbital ellipsis and E denoting the eccentric anomaly. This equation can be solved using the Newton–Raphson method. From E, the true anomaly ν and the distance $R(\nu)$ from the Earth's center can subsequently be derived [9]. It can be seen that the altitude of the satellite relative to the Earth's surface for

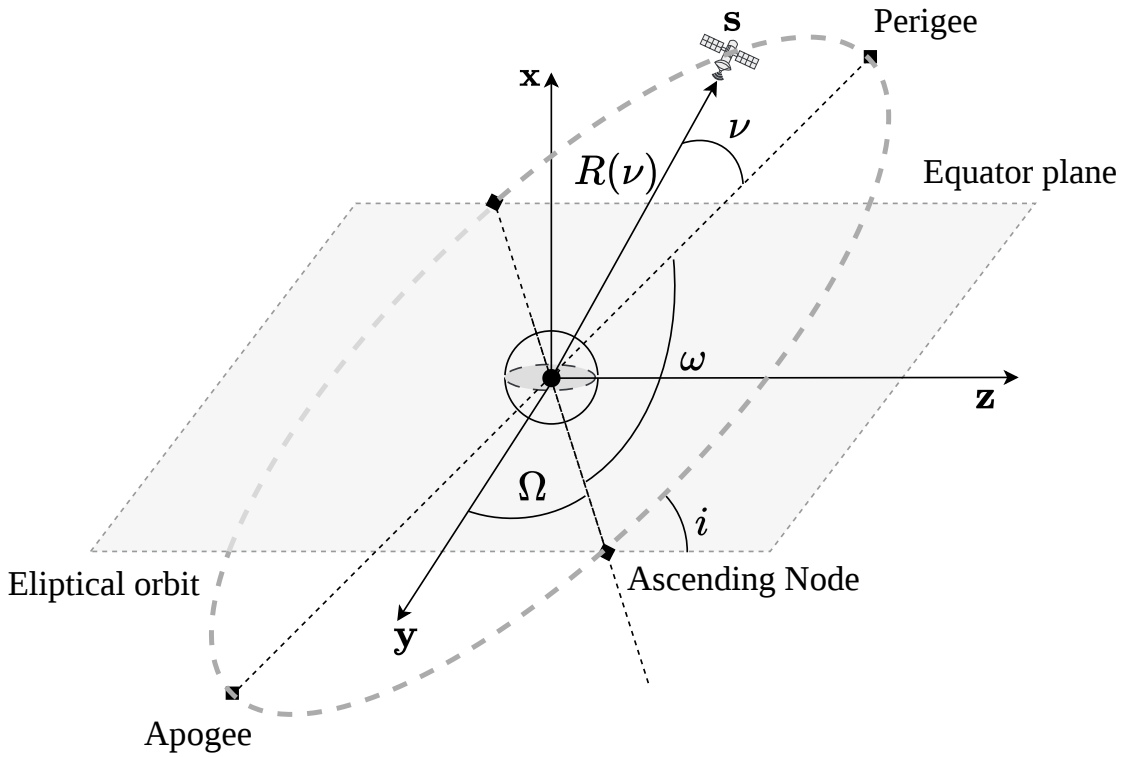

Figure 4.2 – Geometry of the elliptical orbit of the NGSO satellite.

a given ν is $h_{\text{NGSO}} = R(\nu) - R_{\text{e}}$. Accordingly, the satellite position within the orbital plane, expressed in (p,q)-coordinates, is given by

$$\begin{bmatrix} p \\ q \\ 0 \end{bmatrix} = \begin{bmatrix} R(\nu)\cos(\nu) \\ R(\nu)\sin(\nu) \\ 0 \end{bmatrix}. \tag{4.2}$$

Based on the position of the NGSO satellites in the (p,q)-coordinate system, one can determine the three-dimensional position in the global (x,y,z)-coordinate system. This position, referenced to the global coordinates system and represented by the vector $\mathbf{s}$, is calculated by the transformation

$$\mathbf{s} = \begin{bmatrix} x \\ y \\ z \end{bmatrix} = \tilde{\mathbf{R}} \begin{bmatrix} p \\ q \\ 0 \end{bmatrix}, \tag{4.3}$$

in which $\tilde{\mathbf{R}} \in \mathbb{R}^{3\times3}$ is the rotation matrix between the (p,q) and (x,y,z) coordinate systems, as described in Recommendation ITU-R S.1503 [9]. Therefore, the position of the n-th satellite in the NGSO network, written as $\mathbf{s}_n$, is determined using (4.3).

It is assumed that the NGSO system satellites are uniformly distributed along each orbital plane and that the orbital planes themselves are uniformly distributed around the Earth. The angular difference between the longitudes of the ascending nodes Ω of different

planes is $2\pi/N_{\mathrm{p}}$. In turn, the angular difference in the true anomaly ν between satellites in the same plane is $2\pi/N_{\mathrm{sp}}$.

An important question arises regarding how to define an upper bound for the size of an NGSO system, that is, the maximum allowable values for N_{p}, N_{sp} and, consequently, N. There is currently no universally accepted minimum safety separation distance between satellites belonging to the same NGSO system. Nevertheless, [49] reports that, for operational safety, Starlink satellites are typically separated by distances ranging from 100 to 150 km. Taking this into account, a conservative separation distance of 150 km is adopted, both between satellites within the same orbital plane and between adjacent orbital planes. Assuming circular orbits to simplify the analysis, for an orbital altitude of $h_{\mathrm{NGSO}} = 1200$ km, this assumption allows a maximum configuration of $N_{\mathrm{p}} = 317$ orbital planes with $N_{\mathrm{sp}} = 317$ satellites per plane, resulting in a total of $N = 100489$ satellites within a single NGSO system.

In addition, to determine the position of each NGSO satellite, it is also necessary to characterize its antenna radiation pattern. The NGSO satellite antenna is modeled according to (3.3). Fig. 3.2 presents the GSO earth station antenna and the NGSO satellite antenna patterns.

4.1.1 Interference Analysis

The EPFD at a GSO earth station located in the position (i,j) of the GSO coverage footprint is expressed as [48]

$$\mathrm{EPFD}_{(i,j)} = \sum_{n\in\mathcal{S}_{\mathrm{v}}(i,j)}^{N} P_{\mathrm{t}} \frac{G_{\mathrm{tx}}(\varphi_n)}{4\pi d_n^2(i,j)} \frac{G_{\mathrm{rx}}(\varphi'_n)}{\bar{G}_{\mathrm{rx}}}, \tag{4.4}$$

in which, $\mathcal{S}_{\mathrm{v}}(i,j)$ denotes the set of visible NGSO satellites to the corresponding earth station, P_{t} represents the RF power at the input of the antenna of the transmit station for the reference bandwidth $B_{\mathrm{w;ref}}$ and $\bar{G}_{\mathrm{rx}}$ corresponds to the maximum gain of the GSO earth station antenna. The term $d_n(i,j)$ denotes the distance between the GSO earth station and the n-th visible NGSO satellite, computed as $d_n(i,j) = ||\mathbf{s}_n - \mathbf{r}(i,j)||$, as illustrated in Fig. 4.3. The angle φ'_n is defined as the angle between the GSO boresight vector $\mathbf{e}(i,j)$ and the vector $\mathbf{x}_n = \mathbf{s}_n - \mathbf{r}(i,j)$. Conversely, the angle φ_n is defined as the angle between the NGSO boresight vector $\mathbf{b}_n$ and the vector $-\mathbf{x}_n$.

The set of NGSO visible satellites is determined as

$$\mathcal{S}_{\mathrm{v}}(i,j) = \{n \in \{0,1,\cdots,N-1\} | 90^\circ - \angle(\mathbf{r}(i,j),\mathbf{x}_n) > 0\}, \tag{4.5}$$

in which $\angle(\cdot,\cdot)$ represents the angle between two vectors. According to (4.5), a satellite is visible if it is located above the GSO earth station horizon at a position $\mathbf{r}(i,j)$.

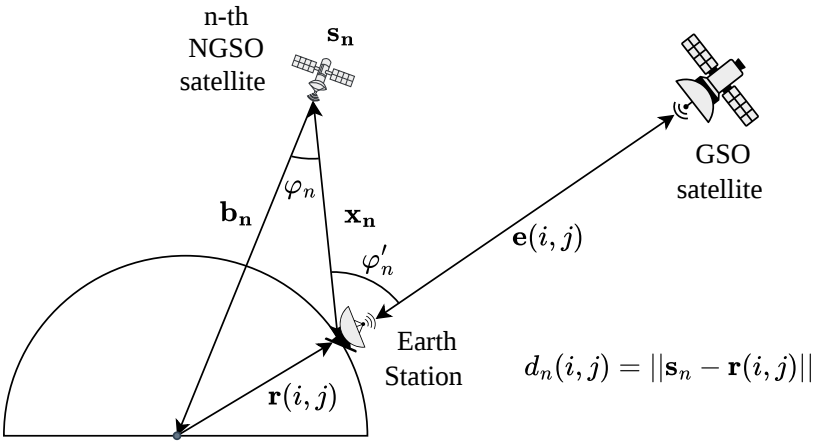

Figure 4.3 – Angles and vectors representation between the NGSO and GSO satellite systems.

4.1.2 Interference Mitigation Techniques

According to Article 22 of the Radio Regulations, the EPFD threshold required to ensure the protection of the GSO system is -160 dB(W/m^2) over a reference bandwidth of 40 kHz. In this study, a conical mitigation zone is defined with an apical half-angle denoted by $\Delta\vartheta$. The PC and BS mitigation techniques are applied to NGSO satellites located within this mitigation cone. Under the PC strategy, NGSO satellites inside the mitigation cone reduce their transmission power by a factor κ. Under the BS strategy, the NGSO antenna pointing angle φ_n is adjusted by a shift $\bar{\varphi}$. Both techniques aim to reduce the interference directed toward GSO earth stations and may be jointly employed within the mitigation region. To guarantee adequate protection of the GSO earth stations, the condition $\Delta\vartheta \geq \Delta\alpha$ must be satisfied. Fig. 4.4 illustrates the interference mitigation zone. For improved practical visualization, Fig. 4.5 depicts a scenario with $N_\mathrm{p} = 20$ orbital planes and $N_\mathrm{sp} = 100$ NGSO satellites per plane, resulting in a total of $N = 2000$ satellites. The GSO satellite provides a footprint with an angular width of $\Delta\alpha = 23.46°$, and a mitigation zone with $\Delta\vartheta = 25°$ is considered, encompassing a total of 73 satellites within the mitigation region.

For a given position $\mathbf{r}(i,j)$, let $\mathcal{S}_\mathrm{a}(i,j) \subset \mathcal{S}_\mathrm{v}(i,j)$ denote the subset of visible NGSO satellites located within the mitigation zone. Accordingly, the EPFD expression in (4.4) can be reformulated to account for the application of the mitigation techniques as

$$\begin{aligned}\mathrm{EPFD}(i,j) = &\sum_{n\in\mathcal{S}_\mathrm{v}(i,j)\setminus\mathcal{S}_\mathrm{a}(i,j)} P_\mathrm{t}\frac{G_\mathrm{tx}(\varphi_n)}{4\pi d_n^2(i,j)}\frac{G_\mathrm{rx}(\varphi'_n)}{\bar{G}_\mathrm{rx}} \\ &+ \sum_{m\in\mathcal{S}_\mathrm{a}(i,j)} (\kappa P_\mathrm{t})\frac{G_\mathrm{tx}(\varphi_m+\bar{\varphi})}{4\pi d_m^2(i,j)}\frac{G_\mathrm{rx}(\varphi'_m)}{\bar{G}_\mathrm{rx}}.\end{aligned} \tag{4.6}$$

In this formulation, the distinction relative to (3.6) in Chapter 3 lies in the fact that the parameters are now expressed as functions of the indices i and j, which correspond to the position of the GSO earth stations in latitude and longitude instead of an angular position α over an arc. Based on this equation, when $\bar{\varphi} = 0$, BS is not implemented. In turn, the

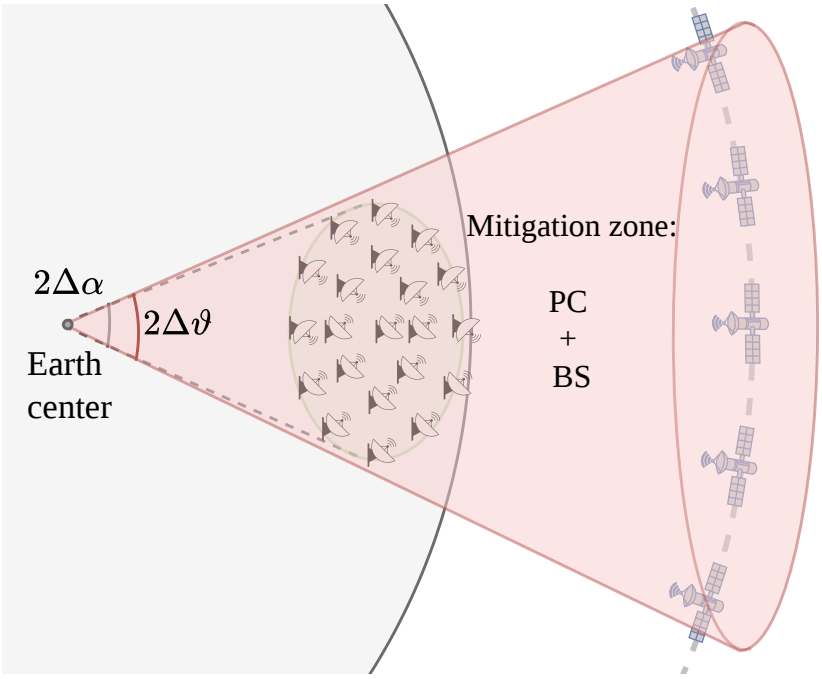

Figure 4.4 – Illustration of the mitigation zone.

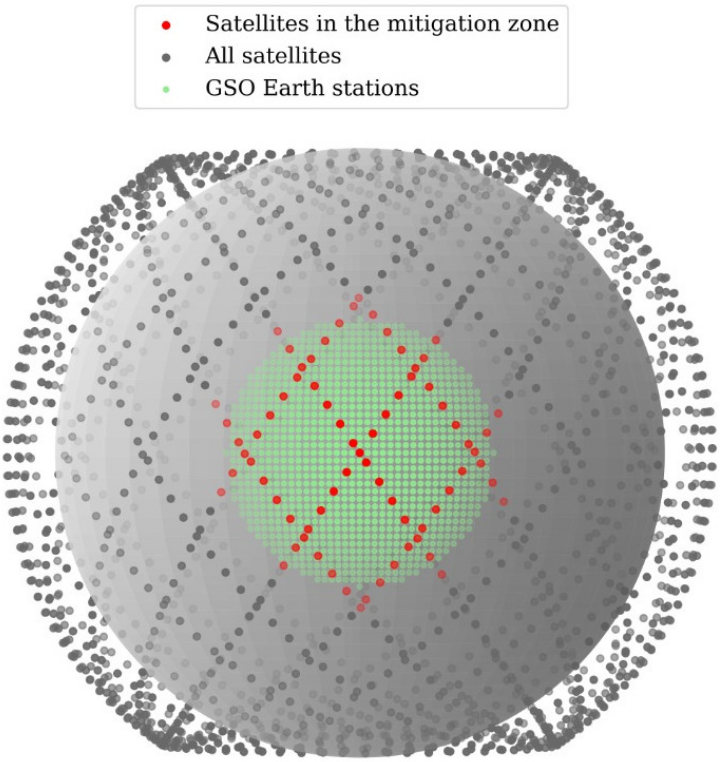

Figure 4.5 – Example of the mitigation zone geometry, showing the GSO footprint ($\Delta\alpha = 23.46°$) and the NGSO satellites contained within the mitigation cone ($\Delta\vartheta = 25°$).

condition $\kappa = 0$ corresponds to the complete deactivation of NGSO satellites operating within the mitigation region.

Table 4.1 – Simulations parameters.

Parameter	Value
Frequency	11.7 GHz
Wavelength – λ	2.56 cm
Reference bandwidth – $B_{\text{w;ref}}$	40 kHz
GSO satellite altitude – h_{GSO}	35786 km
GSO satellite beamwidth – $2\Delta\beta$	8°
Footprint angular width – $2\Delta\alpha$	23.46°
EIRP in the $B_{\text{w;ref}}$	−3.4 dBW
NGSO satellite max. antenna gain – $\bar{G}_{\text{tx}}$	34 dBi
RF power at the input of the NGSO antenna transmit station in the $B_{\text{w;ref}}$ – P_{t}	−37.4 dBW
NGSO Altitude – h_{NGSO}	1200 km
Degree of uniformity of the sidelobes – K	4
Normalized NGSO satellite antenna size – δ_{tx}	11.7
Normalized earth station antenna size – δ_{rx}	23.42

4.2 Numerical Results

This section presents the simulation results[1] of the proposed model in this chapter. The simulations were performed at a frequency of 11.7 GHz, corresponding to a wavelength of $\lambda = 2.56$ cm. The GSO satellite was positioned at an altitude of $h_{\text{GSO}} = 35786$ km and utilized an antenna with an effective beamwidth of $2\Delta\beta = 8°$. By applying (4.1), the resulting satellite footprint corresponds to an angular width of $\Delta\alpha = 23.46°$, measured from the Earth's center. The corresponding footprint has a radius equal to $R_{\text{f}} = 2768$ km. The GSO earth station antennas are assumed to have a normalized aperture size of $\delta_{\text{rx}} = 23.42$ wavelengths, which, according to ITU-R Recommendation S.1428, corresponds to a maximum gain of $\bar{G}_{\text{rx}} = 34.3$ dBi.

The same NGSO parameters and assumptions considered in Chapter 3 were applied in the simulations of this chapter, with a $\delta_{\text{tx}} = 11.7$ due to the change of the frequency band used. For simplicity, we assume that the NGSO satellites are uniformly distributed in circular orbits at a fixed altitude of $h_{\text{NGSO}} = 1200$ km. A summary of the simulation parameters is provided in Table 4.1.

Fig. 4.6 presents the EPFD CDF curves for different sizes of NGSO systems, without any mitigation techniques. Results show that, for relatively small systems with up to $N = 30 \times 317 = 9510$ satellites, the percentage of cases exceeding the EPFD limit remains below 20%. In contrast, for denser NGSO constellations, the impact on the GSO system becomes significantly more severe. In the limiting case with $N = 317 \times 317 = 100489$ satellites (*cf.* Section 4.1), more than 90% of the earth stations experience EPFD levels above the protection

[1] The code is available at: https://github.com/lucianarnf/satsim

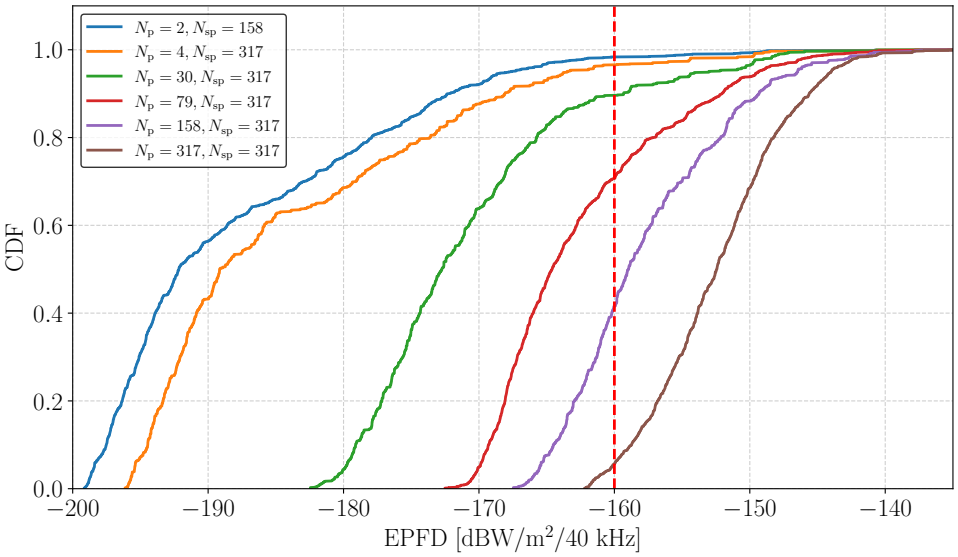

Figure 4.6 – EPFD CDF curves for different NGSO system sizes.

threshold. The findings shown in Fig. 4.6 therefore motivate the adoption of the proposed mitigation techniques, particularly for highly dense deployment scenarios.

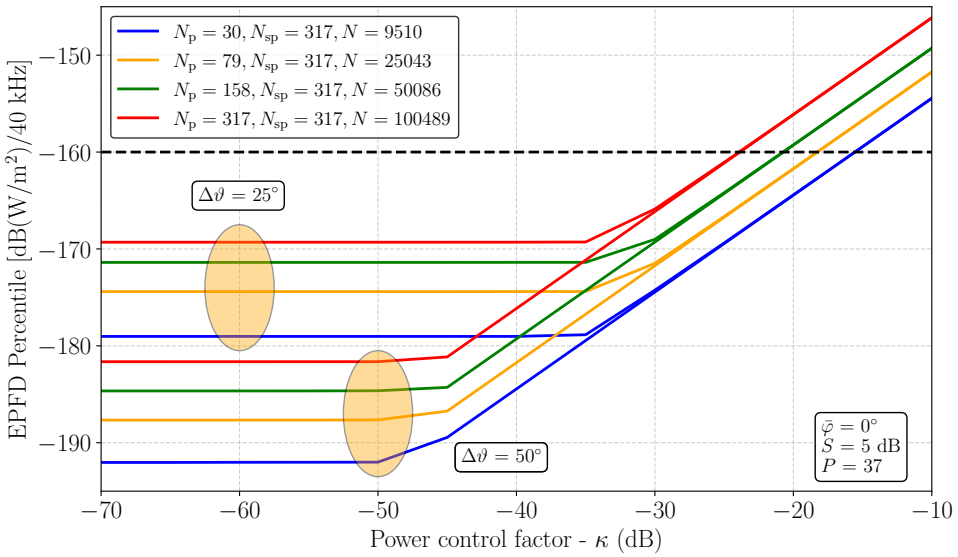

Figure 4.7 – Curves of EPFD 99.9th percentile as a function of the PC coefficient κ (dB), for different NGSO satellite altitudes and mitigation zone widths.

Fig. 4.7 presents the 99.9th percentile of the EPFD as a function of the power control factor κ (in dB), considering 1369 earth stations ($P = 37$), $S = 5$ dB, and no application of beam steering ($\bar{\varphi} = 0°$). Two mitigation zone sizes are evaluated, namely $\Delta\vartheta = 25°$ and $\Delta\vartheta = 50°$. In all considered scenarios, a PC factor of approximately -25 dB is sufficient for the NGSO system to satisfy the EPFD limits in 99.9% of cases. For a fixed mitigation angle $\Delta\vartheta$, reducing the PC factor κ does not necessarily lead to a proportional decrease in the maximum EPFD. This behavior arises because the power constraint is applied only to

satellites located within the mitigation zone. As κ decreases, the system enters in a saturation regime in which the residual interference is predominantly generated by satellites outside the mitigation zone, making further reductions in κ ineffective in lowering the maximum EPFD. The results further indicate that increasing $\Delta\vartheta$ includes a larger number of satellites in the interference mitigation process, which consequently reduces the maximum EPFD over the GSO footprint.

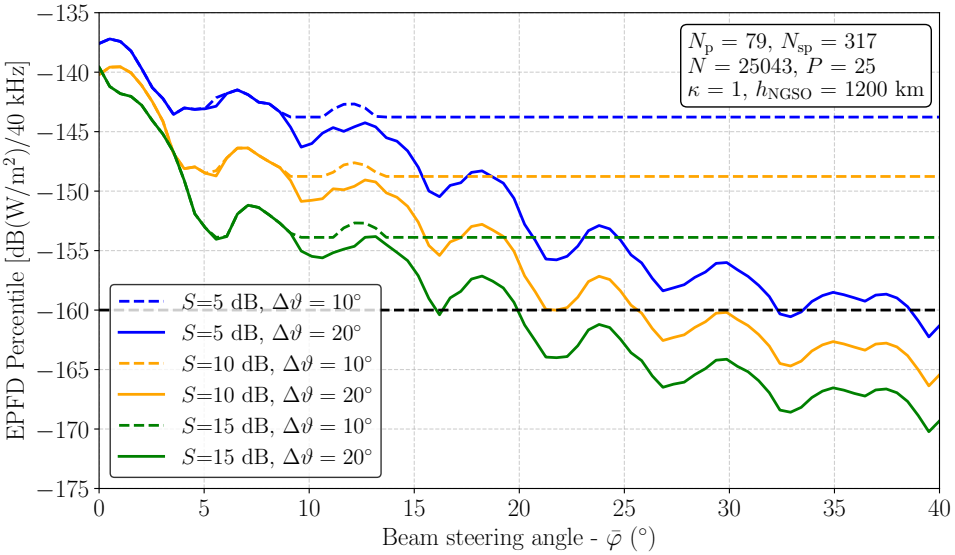

Figure 4.8 – Curves of EPFD 99.9th percentile as a function of the BS angle $\bar{\varphi}$, for different NGSO sidelobe levels and mitigation zone angles.

Fig. 4.8 presents the 99.9th percentile of the EPFD as a function of the BS deviation angle $\bar{\varphi}$ for different sidelobe levels S and mitigation zones $\Delta\vartheta$. The results consider $N_p = 79$ orbital planes with $N_{sp} = 317$ satellites per plane, resulting in a total of $N = 25043$ satellites. Power control mitigation is not applied ($\kappa = 1$). First, it is observed that when $\Delta\alpha \ll \Delta\vartheta$ with $\Delta\vartheta = 10°$, there exists a value of $\bar{\varphi}$ beyond which the percentile no longer decreases. At this point, the interference becomes dominated by satellites located outside the mitigation zone. Conversely, when $\Delta\alpha \approx \Delta\vartheta$ with $\Delta\vartheta = 20°$, increasing the BS deviation angle preserves the decreasing trend of the EPFD percentile. For the case $S = 15$ dB, 99.9% of the realizations are protected for a deviation of approximately $\bar{\varphi} = 20°$. The influence of the sidelobe level is also significant: as S decreases, the effectiveness of the BS technique reduces. This behavior is attributed to the higher power radiated through the secondary lobes, which sustains substantial interference levels even for relatively large deviation angles $\bar{\varphi}$.

For improved visualization of the spatial distribution of interference, EPFD heat maps were developed. First, Fig. 4.9 shows the heat map without the application of mitigation techniques. Elevated interference levels are observed in the central region, primarily due to the geometric alignment between the earth stations—whose antennas are oriented toward the GSO satellite—and the NGSO satellite beams, which are directed toward nadir. The

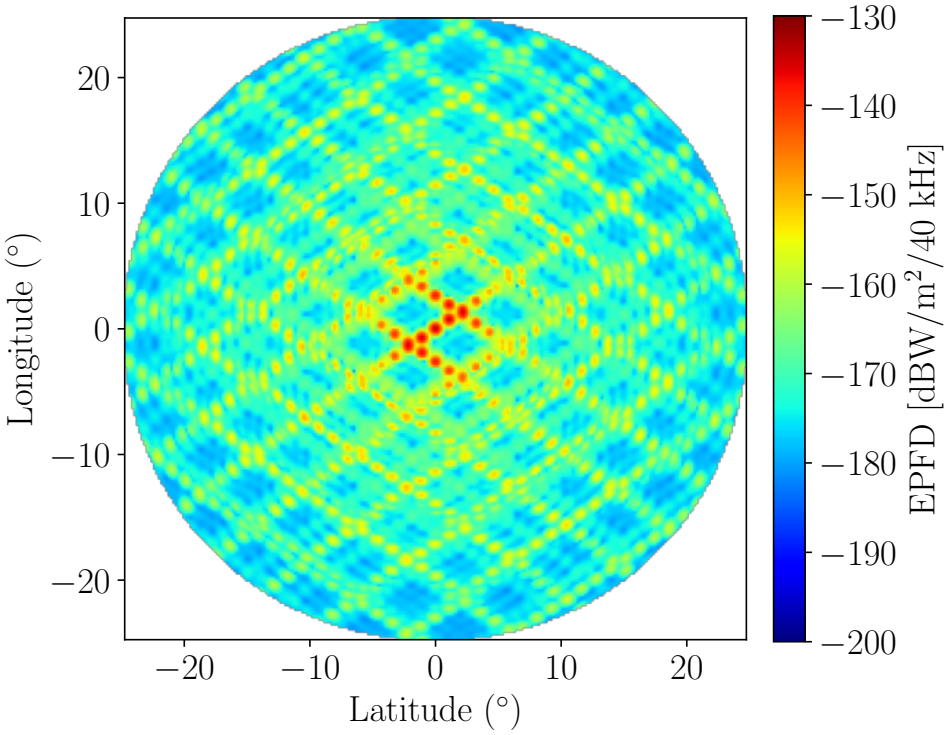

Figure 4.9 – EPFD heat map for $N_p = 79$, $N_{sp} = 317$, $N = 25043$, P=256, $S = 15$ dB, disregarding the mitigation techniques, *i.e.*, $\kappa = 1$ and $\bar{\varphi} = 0°$.

checkerboard pattern visible in this figure arises from the intersections of the NGSO orbital planes. In turn, Fig. 4.10 presents the same scenario with the application of the PC technique using $\kappa = -25$ dB. An overall reduction in the EPFD level is observed, with a large portion of the footprint experiencing interference levels below -160 dBW/m^2/40 kHz. Finally, Fig. 4.11 shows the case in which the BS technique is applied with a beam deviation of $\bar{\varphi} = 20°$. A less pronounced reduction is obtained compared to the PC case; nevertheless, a considerable performance improvement is still achieved relative to the scenario without mitigation. These results demonstrate that both PC and BS mitigation techniques can be effectively employed to reduce interference under the specified conditions.

Finally, Fig. 4.12 presents the EPFD CDF curves for different interference mitigation configurations. The simulations consider an NGSO system with $N = 25043$ satellites, a mitigation angle of $\Delta\vartheta = 25°$, and a sidelobe level of $S = 15$ dB. As a benchmark, the EPFD CDF corresponding to the case without any mitigation technique is also shown. In this scenario, approximately 30% of the cases exceed the EPFD protection limit. For all analyzed configurations, the joint application of PC and BS proves effective in achieving EPFD levels below the ITU-R threshold, while requiring less severe individual mitigation levels than those needed when each technique is applied independently. These results indicate that the combined use of PC and BS constitutes an efficient interference mitigation strategy and can be implemented in a manner that does not significantly compromise the operational domain of the NGSO system.

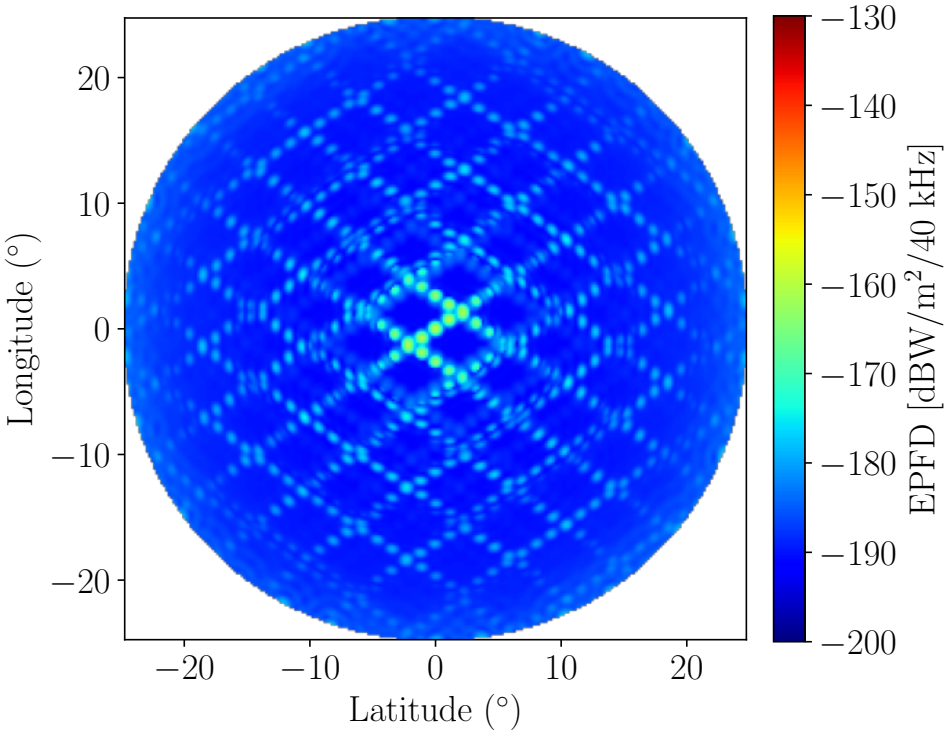

Figure 4.10 – EPFD heat map for $N_p = 79$, $N_{sp} = 317$, $N = 25043$ and $S = 15$ dB, considering PC solely, with κ = -25 dB.

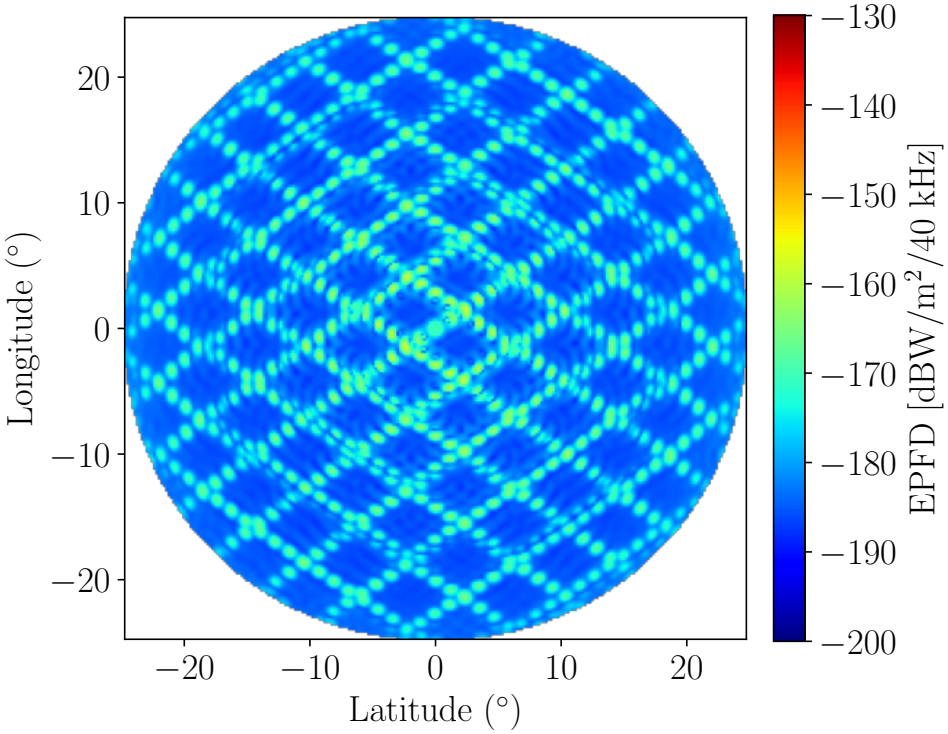

Figure 4.11 – EPFD heat map for $N_p = 79$, $N_{sp} = 317$, $N = 25043$ and $S = 15$ dB, considering BS solely, with $\bar{\varphi} = 20°$.

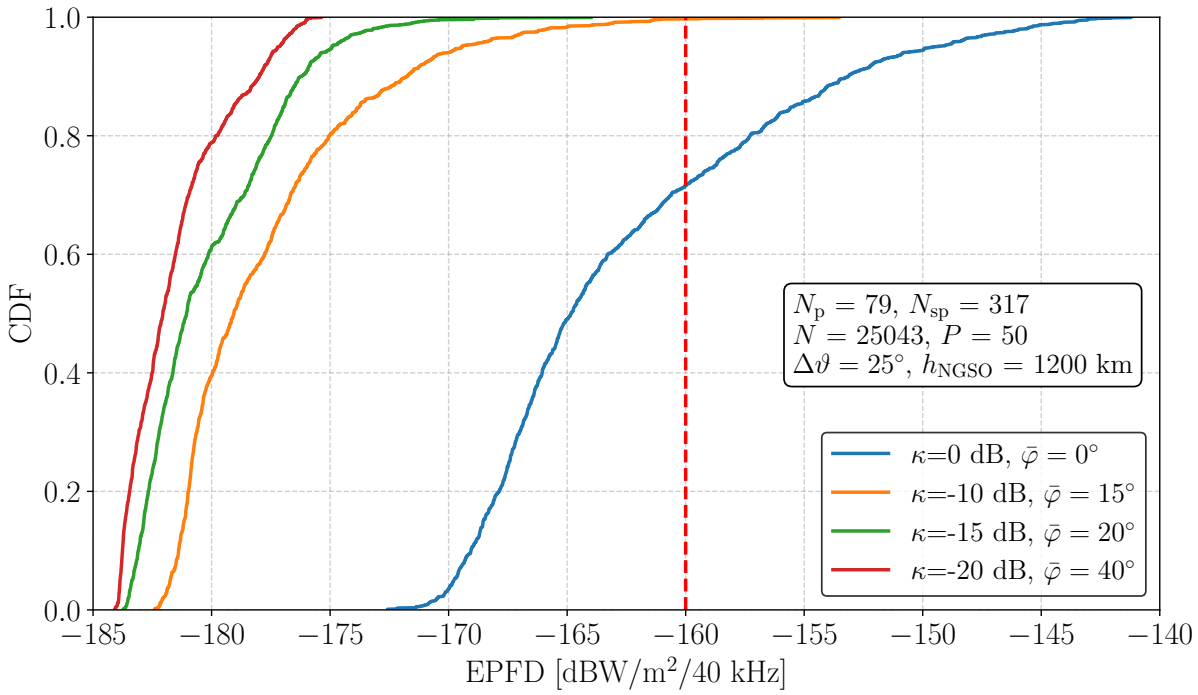

Figure 4.12 – Resulting EPFD CDF curves for the joint application of PC (κ) and BS ($\bar{\varphi}$).

4.3 Conclusions

This chapter analyzed the coexistence between NGSO and GSO satellite systems in the Ku band. A simulation framework aligned with ITU recommendations was used to assess EPFD levels under more realistic conditions, including large NGSO systems with multiple orbital planes. The results indicated that smaller systems may naturally comply with EPFD limits due to the limited number of simultaneously visible satellites, whereas large systems significantly increase the probability of harmful interference, making mitigation techniques necessary.

The study demonstrated that, although PC and BS individually provide limited benefits in certain scenarios, their combined use effectively reduces interference and ensures compliance with regulatory limits, particularly in NGSO directive antennas. Spatial analyses confirmed substantial EPFD reductions across the GSO coverage area, even for very large systems.

5 Conclusions

This dissertation addressed one of the most pressing challenges in contemporary satellite communications: ensuring the spectral coexistence between NGSO systems and GSO systems operating in the Ku band. With the rapid expansion of large-scale NGSO systems and the increasing congestion of the geostationary arc, interference mitigation has become a critical requirement to guarantee regulatory compliance and the sustainable growth of multi-orbit satellite networks.

A comprehensive review of the state of the art was first conducted, covering both non-cooperative and cooperative interference mitigation strategies, as well as emerging interference detection techniques based on machine learning and AI. This survey highlighted that, although numerous solutions have been proposed—such as exclusion angles, PC, beamforming, dynamic spectrum access, and cognitive radio—no single technique consistently satisfies the stringent EPFD limits established by the ITU under WCG, particularly in dense NGSO deployment scenarios.

Motivated by these limitations, this work proposed and evaluated a joint interference mitigation strategy based on the combined application of PC and BS within a predefined angular mitigation zone. Unlike approaches that require tight coordination or complex signaling between systems, the proposed method relies exclusively on geometric parameters known a priori by both NGSO and GSO systems. This characteristic makes the solution suitable for real-world implementation.

In Chapter 3, a simplified system model was introduced to analytically investigate the impact of the joint PC and BS strategy. Closed-form expressions were derived, including a modified EPFD formulation that incorporates both mitigation techniques. Numerical results suggested that applying PC or BS individually is generally insufficient to meet ITU EPFD limits under WCG conditions. However, their combined use significantly reduces interference levels, enabling compliance while preserving NGSO service availability.

Chapter 4 extended the analysis to a more realistic scenario, incorporating NGSO satellite positions defined according to ITU-R recommendations and a GSO footprint area in which earth stations are distributed. Even under these more complex and practical conditions, the joint mitigation approach proved effective in controlling the 99.9th percentile EPFD and ensuring regulatory compliance across a wide range of system parameters, including NGSO system size, altitude, sidelobe levels, and mitigation zone width. The results confirm that the synergy between PC and BS provides a robust and flexible mechanism to balance interference protection and system performance.

Overall, the main contributions of this dissertation could be summarized as:

- The development of a low-complexity method that jointly applies PC and BS mitigation strategies within a defined angular mitigation zone in the Ku band.
- An expression that defines the equivalent angle at Earth's center of the GSO satellite antenna beam width.
- The derivation of analytical expressions adapting the EPFD formulation to incorporate mitigation mechanisms.
- The validation of the proposed approach under both simplified and more realistic system models, considering WCG and real NGSO system parameters.
- The demonstration that joint mitigation is essential to satisfy ITU regulatory constraints in dense multi-orbit environments.

In conclusion, this work demonstrated that the coordinated application of PC and BS within a well-defined mitigation zone constitutes an effective and implementable solution for protecting GSO systems from NGSO interference in shared Ku-band scenarios. As satellite communications evolve toward increasingly integrated multi-orbit architectures and tighter spectrum reuse, such joint and geometry-aware mitigation strategies will play a fundamental role in enabling resilient, efficient, and sustainable global connectivity.

Future work may extend the proposed framework by incorporating the dynamic nature of NGSO constellations, enabling time-varying analysis of interference and system performance. Additionally, the impact of mitigation strategies on user-centric quality of service metrics, such as throughput and latency, should be investigated. The integration of cooperative approaches, including CR, DSA, and RIS-assisted communications, also represents a promising research direction. Furthermore, the analysis of aggregate interference from multiple NGSO systems remains an open challenge, particularly in the context of current regulatory limitations. The adoption of machine learning techniques for adaptive interference management, as well as the investigation of practical implementation aspects and real-time interference measurement, are also relevant topics for future studies. Finally, extending the proposed framework to higher frequency bands and hybrid satellite–terrestrial networks may contribute to the development of next-generation multi-orbit communication systems.

References

[1] SPACENEWS. **Orbital congestion reaching critical levels, warns new report**. 2025. Disponível em: https://spacenews.com/orbital-congestion-reaching-critical-levels-warns-new-report/. Cit. on p. 17.

[2] ITU-R. **Radio Regulations**. [S.l.]: ITU-R, 2024. Cit. on p. 17.

[3] SATELLITE, V. **Satellite Issues Take Center-Stage at WRC-23**. 2025. Disponível em: https://interactive.satellitetoday.com/via/january-february-2024/satellite-issues-take-center-stage-at-wrc-23. Cit. on p. 17.

[4] BRAUN, e. a. C. Should we worry about interference in emerging dense NGSO satellite constellations? **IEEE International Symposium on Dynamic Spectrum Access Networks**, p. 1–10, 2019. Cit. on p. 17.

[5] WANG, e. a. H. Coexistence downlink interference analysis between LEO system and GEO system in Ka band. **IEEE International Conference on Communications in China**, p. 465–469, 2018. Cit. on p. 17.

[6] HILLS, e. a. A. Feasibility of using beam steering to mitigate Ku-Band LEO-to-GEO interference. **IEEE Access**, v. 10, p. 74023–74032, 2022. Cit. on p. 17.

[7] HILLS, e. a. A. Controlling antenna sidelobe radiation to mitigate ku-band LEO-to-GEO satellite interference. **IEEE Access**, v. 11, p. 71154–71163, 2023. Cit. on p. 17.

[8] HUANG, e. a. Y. Co-frequency interference analysis between ultra-large-scale NGSO constellations and gso systems. **Journal of Communications and Information Networks**, v. 8, p. 80–89, 2023. Cit. on p. 17.

[9] ITU-R. Recommendation ITU-R S.1503-4 - functional description to be used in developing software tools for determining conformity of non-geostationary-satellite orbit fixed-satellite service systems or networks with limits contained in article 22 of the radio regulations. **Int. Telecommun. Union**, Geneva, Switzerland, 2023. Cit. on pp. 18, 47 e 48.

[10] WANG, H.; WANG, C.; YUAN, J.; ZHAO, Y.; DING, R.; WANG, W. Coexistence downlink interference analysis between LEO system and GEO system in Ka band. In: **Proc. of IEEE International Conference on Communications in China**. [S.l.: s.n.], 2018. p. 465–469. Cit. on p. 20.

[11] POLO, E.; EMILIANI, L.; LUINI, L. Investigating the interference induced by NGSO constellations on GSO system ground stations: A simulation approach. In: **Proc. of 18th European Conference on Antennas and Propagation**. Glasgow, United Kingdom: [s.n.], 2024. p. 1–5. Cit. on p. 22.

[12] JALALI, M.; ORTIZ, F.; LAGUNAS, E.; KISSELEFF, S.; EMILIANI, L.; CHATZINOTAS, S. Joint power and tilt control in satellite constellation for NGSO-GSO interference mitigation. **IEEE Open Journal of Vehicular Technology**, v. 4, p. 545–557, ago. 2023. Cit. on pp. 22 e 26.

[13] POURMOGHADAS, A.; SHARMA, S. K.; CHATZINOTAS, S.; OTTERSTEN, B. On the spectral coexistence of GSO and NGSO FSS systems: power control mechanisms and a methodology for inter-site distance determination. **International Journal of Satellite Communications and Networking**, v. 35, n. 5, p. 443–459, nov. 2016. Cit. on pp. 22 e 32.

[14] ZHANG, X.; TONG, J.; REN, Y. Power allocation for multi-satellite system integrated with precoding and user scheduling. In: **Proc. of 8th International Conference on Electronics Information and Emergency Communication**. Beijing, China: [s.n.], 2018. p. 170–174. Cit. on p. 22.

[15] JALALI, M.; LAGUNAS, E.; HAQIQATNEJAD, A.; KISSELEFF, S.; CHATZINOTAS, S. Downlink beamforming strategies for interference-aware NGSO satellite systems. **IEEE Open Journal of the Communications Society**, v. 5, p. 3468–3483, maio 2024. Cit. on p. 23.

[16] LAGUNAS, E.; PEREZ-NEIRA, A.; GROTZ, J.; CHATZINOTAS, S.; OTTERSTEN, B. Beam splash mitigation for NGSO spectrum coexistence between feeder and user downlink. In: **Proc. of WSA & SCC 2023; 26th International ITG Workshop on Smart Antennas and 13th Conference on Systems, Communications, and Coding**. Braunschweig, Germany: [s.n.], 2023. p. 1–6. Cit. on p. 23.

[17] JALALI, M.; ORTIZ, F.; LAGUNAS, E.; KISSELEFF, S.; CHATZINOTAS, S.; EMILIANI, L. LEO satellite beamforming for NGSO-GSO interference mitigation. In: **Proc. of 40th International Communications Satellite Systems Conference**. Bradford, UK: [s.n.], 2023. p. 169–175. Cit. on p. 23.

[18] GUO, H.; HUANG, W.; WANG, W.; GUO, J.; QIU, Z. An interference mitigation strategy for LEO satellite systems based on adaptive beamforming with sidelobe suppression. In: **Proc. of 19th International Conference on Mobility, Sensing and Networking**. Nanjing, China: [s.n.], 2023. p. 135–142. Cit. on p. 23.

[19] WANG, H.; ZOU, C.; SHAO, F.; CHANG, J.; HUANG, C.; LI, G. Collinear interference avoidance strategy for LEO satellite constellation based on transmit beamforming. **IEICE Transactions on Communications**, p. 1–16, 2025. Cit. on p. 24.

[20] ZHANG, C.; JIN, J.; ZHANG, H.; LI, T. Spectral coexistence between LEO and GEO satellites by optimizing direction normal of phased array antennas. **China Communications**, v. 15, n. 6, p. 18–27, jun. 2018. Cit. on p. 24.

[21] ZUO, S. et al. Movable antenna-aided interference mitigation for LEO-GEO spectrum-sharing system. In: **Proc. of IEEE Wireless Communications and Networking Conference**. [S.l.: s.n.], 2025. p. 1–6. Cit. on p. 24.

[22] ZHU, L.; PI, X.; MA, W.; XIAO, Z.; ZHANG, R. Dynamic beam coverage for satellite communications aided by movable-antenna array. **IEEE Transactions on Wireless Communications**, v. 24, n. 3, p. 1916–1933, mar. 2025. Cit. on p. 24.

[23] ZHU, L.; PI, X.; MA, W.; XIAO, Z.; ZHANG, R. Movable antenna aided satellite beam coverage optimization. In: **Proc. of IEEE Global Communications Conference (GLOBECOM)**. Cape Town, South Africa: [s.n.], 2024. p. 2575–2580. Cit. on p. 24.

[24] HSU, Y.-H.; LEE, J.-I.; HUANG, L.-Y.; HSIAO, W.-L. A DRL-Based spectrum-sharing scheme for GEO-LEO co-existing satellite networks. In: **Proc. of IEEE Vehicular Technology Conference**. [S.l.: s.n.], 2024. p. 1–5. Cit. on p. 25.

[25] YUN, J.; KU, B.-J.; OH, D.; JOO, C. Hierarchical learning for interference management in multi-user LEO satellite networks. **Journal of Communications and Networks**, v. 27, n. 2, p. 119–126, abr. 2025. Cit. on p. 25.

[26] HILLS, A.; PEHA, J. M.; MUNK, J.; POGORELC, S. Controlling antenna sidelobe radiation to mitigate Ku-Band LEO-to-GEO satellite interference. **IEEE Access**, v. 11, p. 71154–71163, jul. 2023. Cit. on pp. 26 e 41.

[27] FERREIRA, L. R. N. et al. Joint power control and beam steering for NGSO-to-GSO interference mitigation in Ku band. In: **SBMO/IEEE MTT-S International Microwave and Optoelectronics Conference (IMOC)**. [S.l.: s.n.], 2025. p. 1–6. Cit. on pp. 26 e 46.

[28] ZHAO, D.; SONG, B.; DU, X. Joint beam management and resource allocation in a GEO and LEO spectrum-sharing system for effective interference avoidance. **IEEE Transactions on Cognitive Communications and Networking**, v. 11, n. 4, p. 2662–2675, ago. 2025. Cit. on p. 26.

[29] ZHENG, Z.; JING, W.; LU, Z.; WEN, X.; LI, W. RIS-aided leo satcom with LEO-GEO inter-system interference mitigation: Joint multi-satellite multi-ris beamforming. In: **Proc. of IEEE Wireless Communications and Networking Conference**. [S.l.: s.n.], 2024. p. 1–6. Cit. on p. 29.

[30] ZHENG, Z.; JING, W.; LU, Z.; WU, Q.; ZHANG, H.; GESBERT, D. Cooperative multi-satellite and multi-RIS beamforming: Enhancing LEO satcom and mitigating LEO-GEO intersystem interference. **IEEE Journal on Selected Areas in Communications**, v. 43, n. 1, p. 279–296, jan. 2025. Cit. on p. 29.

[31] NGO, Q. T.; PHAN, K. T.; MAHMOOD, A.; XIANG, W. DRL-based secure beamforming for hybrid-RIS aided satellite downlink communications. In: **Proc. of IEEE Interna-**

tional Conference on Communication, Networks and Satellite. Solo, Indonesia: [s.n.], 2022. p. 432–437. Cit. on p. 30.

[32] KAMAL, M. M. et al. Secure satellite downlink with hybrid RIS and AI-based optimization. **IEEE Access**, v. 13, p. 3726–3737, 2025. Cit. on p. 30.

[33] KHAN, W. U.; LAGUNAS, E.; MAHMOOD, A.; CHATZINOTAS, S.; OTTERSTEN, B. RIS-assisted energy-efficient LEO satellite communications with NOMA. **IEEE Transactions on Green Communications and Networking**, v. 8, n. 2, p. 780–790, jun. 2024. Cit. on p. 30.

[34] IEEE. **IEEE Draft Standard Definitions and Concepts for Dynamic Spectrum Access: Terminology Relating to Emerging Wireless Networks, System Functionality, and Spectrum Management**. [S.l.], 2018. 1–76 p. Cit. on p. 30.

[35] LI, B.; PARK, J.; AL-HOURANI, A.; POKHREL, S. R.; CHOI, J. A novel frequency reuse model for co-existing LEO and GEO satellites. **IEEE Wireless Communications Letters**, v. 13, n. 4, p. 1024–1028, abr. 2024. Cit. on p. 30.

[36] RYU, J.; KAUSHIK, A.; LEE, B.; SHIN, W. Rate-splitting multiple access for GEO-LEO coexisting satellite systems: A traffic-aware throughput maximization precoder design. **IEEE Transactions on Vehicular Technology**, v. 73, n. 12, p. 19838–19843, dez. 2024. Cit. on pp. 31 e 32.

[37] GU, P.; LI, R.; HUA, C.; TAFAZOLLI, R. Cooperative spectrum sharing in a co-existing LEO-GEO satellite system. In: **Proc. of IEEE Global Communications Conference**. [S.l.: s.n.], 2020. p. 1–6. Cit. on p. 31.

[38] GU, P.; LI, R.; HUA, C.; TAFAZOLLI, R. Dynamic cooperative spectrum sharing in a multi-beam LEO-GEO co-existing satellite system. **IEEE Wireless Communications Letters**, v. 21, n. 2, p. 1170–1182, fev. 2022. Cit. on p. 32.

[39] YANG, R.; DAI, S.; WANG, P.; YE, J. Power optimization for spectral efficiency maximization in cognitive radio GEO-LEO co-existing satellite networks. In: **Proc. of International Conference on Intelligent Communication and Networking**. [S.l.: s.n.], 2024. p. 13–19. Cit. on p. 32.

[40] SAIFALDAWLA F. ORTIZ, E. L. A. B. M. A. A.; CHATZINOTAS, S. GenAI-based models for NGSO satellites interference detection. **IEEE Trans. Mach. Learn. Commun. Netw.**, v. 2, p. 904–924, 2024. Cit. on pp. 32 e 33.

[41] SAIFALDAWLA, A.; ORTIZ-GOMEZ, F. G.; LAGUNAS, E.; DAOUD, S.; CHATZINOTAS, S. NGSO-To-GSO satellite interference detection based on autoencoder. In: **Proc. of International Symposium on Personal, Indoor and Mobile Radio Communications**. [S.l.: s.n.], 2023. p. 1–7. Cit. on p. 33.

[42] SAIFALDAWLA F. ORTIZ, E. L. A.; CHATZINOTAS, S. Convolutional autoencoders for non-geostationary satellite interference detection. **IEEE International Conference on Communications Workshop**, Denver, CO, USA, p. 1334–1339, 2024. Cit. on p. 34.

[43] DAOUD G. EAPPEN, F. O. E. L. W. M. S.; CHATZINOTAS, S. CNN-based on-board interference detection in satellite systems: An analysis of dataset impact on performance. **IEEE International Conference on Acoustics, Speech, and Signal Processing Workshops**, Rhodes Island, Greece, p. 1–5, 2023. Cit. on p. 34.

[44] TAYLOR, T. Design of circular apertures for narrow beamwidth and low sidelobes. **IRE Transactions on Antennas and Propagation**, v. 8, p. 17–22, 1960. Cit. on p. 38.

[45] ITU-R. Recommendation ITU-R S.1528-0 - satellite antenna radiation patterns for non-geostationary orbit satellite antennas operating in the fixed-satellite service below 30 ghz. **Int. Telecommun. Union**, Geneva, Switzerland, 2001. Cit. on p. 38.

[46] AGENCY, E. S. R23-WP4A-C-0466!!MSW-E - working document towards a preliminary draft new revision of Recommendation ITU-R S.1528. **Int. Telecommun. Union**, Geneva, Switzerland, 2025. Cit. on p. 38.

[47] ITU-R. Recommendation ITU-R S.1428-1 - reference fss earth-station radiation patterns for use in interference assessment involving non-gso satellites in frequency bands between 10.7 ghz and 30 ghz. **Int. Telecommun. Union**, Geneva, Switzerland, 2001. Cit. on pp. 39 e 47.

[48] JALALI, M. e. a. Joint power and tilt control in satellite constellation for NGSO-GSO interference mitigation. **IEEE Open Journal of Vehicular Technology**, v. 4, p. 545–557, 2023. Cit. on pp. 39 e 49.

[49] MARSHALL, G. C. **The Placement of Satellites in SpaceX's Starlink Mission Play an Important Role in its Fast Internet Speed**. TechRxiv, 2024. Cit. on p. 49.


UnB